ΠΑΝΕΠΙΣΤΗΜΙΟ ΚΥΠΡΟΥ

Διατριβή Μάστερ

FORGING OF MULTI-METAL GEARS

Λυσιμάχη Ιωνά

ΤΜΗΜΑ ΜΗΧΑΝΙΚΩΝ ΜΗΧΑΝΟΛΟΓΙΑΣ ΚΑΙ ΚΑΤΑΣΚΕΥΑΣΤΙΚΗΣ

ΜΑΪΟΣ 2023

ΠΑΝΕΠΙΣΤΗΜΙΟ ΚΥΠΡΟΥ
ΤΜΗΜΑ ΜΗΧΑΝΙΚΩΝ ΜΗΧΑΝΟΛΟΓΙΑΣ
ΚΑΙ ΚΑΤΑΣΚΕΥΑΣΤΙΚΗΣ

Forging of multi-metal gears

Λυσιμάχη Ιωνά

Επιβλέπων Καθηγητής
Δρ. Ντένις Πολίτης

Η Διατριβή Μάστερ υποβλήθηκε προς μερική εκπλήρωση των απαιτήσεων απόκτησης του μεταπτυχιακού MSc. Μηχανικού Μηχανολογίας και Κατασκευαστικής του Τμήματος Μηχανικών Μηχανολογίας και Κατασκευαστικής

Μάιος 2023

Ευχαριστίες

Θα ήθελα να ευχαριστήσω τον επιβλέποντα καθηγητή μου Δρ. Ντένις Πολίτη του τμήματος Μηχανικών Μηχανολογίας και Κατασκευαστικής για την καθοδήγηση, και κυρίως για την εμπιστοσύνη που μου έδειξε κατά τη διάρκεια διεκπεραίωσης της διπλωματικής μου εργασίας.

Επιπρόσθετα, θα ήθελα να ευχαριστήσω τον κ. Πέτρο Βενεκτή που μου επέτρεψε να χρησιμοποιήσω τον εξοπλισμό των εργαστηρίων και συνέδραμε καταλυτικά για την κατασκευή μερών που χρησιμοποιήθηκαν στην παρούσα εργασία.

Ιδιαίτερες ευχαριστίες στην οικογένεια και τους φίλους μου για την στήριξη και την κατανόηση που έδειξαν τόσο αυτή τη χρονιά, όσο και κατά τη διάρκεια των σπουδών μου.

Abstract

Material substitution is becoming increasingly popular in the transport sector, since the reduction of emissions is closely linked to the reduction of vehicular weight. In the case of gears, the aim is to reduce the gearbox assembly weight with the manufacturing of light-weight gears made of multiple metals, instead of conventional ones made of steel. In this thesis, different material combinations are tested to produce a 13-teeth spur gear with forging. The intermetallic bond between the dissimilar metals is also observed, to determine the gear's performance. From the experimental results, it was noted that there was no sufficient deformation of the gears due to the inadequate capacity of the hydraulic press. In addition, the forging conditions were not beneficial for a successful bond between the dissimilar metals, in most cases. Only two gear samples were found to be bonded, however in one case there was a visible gap between the different metals, while in the other one, when observed under an optical microscope clear boundaries of the materials signified that the experimental conditions were not favorable for diffusion.

Table of Contents

Figures

Appendices

Chapter 1

1 INTRODUCTION

1.1 Motivation

Gears used in various industries, such as automotive and aerospace, often require lightweight components to improve overall system efficiency and fuel economy. Multi-metal gears offer the opportunity to reduce weight, by selectively using lightweight metals or alloys in non-critical areas. However, reducing the weight of gears while maintaining strength and durability remains a challenge. Further investigation is required in how to achieve a high-quality intermetallic bond between the dissimilar metals and whether the multi-metal gears would perform as good as single material gears in real life applications. This thesis focuses on the manufacturing of a multi-metal 13-teeth spur gear and whether a successful material bonding is achieved.

1.2 Manufacturing Technologies

There are various techniques used to achieve weight reduction in gears. One commonly used method is machining thin webs in low-stress regions of gears [[1], [2]], but this approach can lead to reduced stiffness and increased bending and contact stresses [3]. Another strategy is material substitution as a means of reducing weight. Manufacturing techniques such as casting follow this strategy, but they have limitations when dealing with materials of substantially differing melting temperatures.

To simplify the manufacturing process, alternative approaches, such as mechanical fastening, welding, or press fitting to assemble gears made from different materials are investigated. However, forging is the most favorable method for producing gears with optimal mechanical properties, since forged components have shown increased impact strength and fatigue life [4] compared to machined parts. The use of forging for bi-metal gear production has been explored, including the production of spur gears, bevel gears

[5], and helical gears [6] through forging techniques. The advantages of forging include reduced post-processing, improved mechanical performance, quick production, higher productivity, and lower costs.

In order to achieve identical performance qualities while reducing total weight, the work described attempts to evaluate the viability of creating bi-metal gears through forging. Forging is a viable method for producing bi-metal gears because to its benefits in terms of material flow, fiber orientation, and cost effectiveness.

Figure 1: Machined gear [7]

Figure 1: Welding of spur and helical gear [8]

1.3 Preform Production

In most studies a conventional forging press is used for forging multi-metal gears, with the manufacturing of the different metal blanks being the main point of distinction. The production methods that are employed are listed below:

1. Production of a single cast preform: Centrifugal casting is used to produce a multi-metal workpiece [9], where tin bronze and yellow brass, two metals with similar melting temperatures, are used as outer and inner materials, respectively. Then, the outer material is machined to form the gear teeth. This method reduces material handling operations, however when using alternative preforms such as aluminium and steel, may result in inconsistencies in the interlayer surface due to the solidification of the outer steel prior to aluminium.

2. Co-extrusion of inner bar and outer sleeve: Co-extrusion of dissimilar metals [10] can be performed at cold or elevated temperatures, with elevated temperatures allowing for welding at the interface. Aluminium-titanium co-extrusion [11] is suggested for lightweight high-strength preforms, as no intermetallic phases or oxygen-contamination result in a robust bond. Backward extrusion of a steel sleeve with an aluminium core [12] was also researched, with the metallurgical bonding being relatively weak, but it could be improved through micro fitting using a sand blasted surface.

3. Shrink fitting technique: Shrink fitting is commonly used for bi-metal assembly. Knurled interference fits of a shape profile [[13], [14] were found to perform better than ordinary interference fits. These findings could also be applied for the production of lightweight multi-metal gears.

4. Welding methods: Deposition welding, laser deposition welding, electromagnetic pulse welding and friction welding were investigated. Deposition welding of a cylindrical base preform coated with a dissimilar metallic layer was found to have a contour with a jagged edge that remained after forging it to a bevel gear [15]. Laser hot-wire cladding and friction welding showed successful bonding, but it was noticed that there was non-uniform distribution of material in the final geometry [16] and presence of an air gap [17] between the two materials, respectively.

5. Forging of un-bonded preforms: Assembly of an outer high-strength ring and an inner cylindrical core material that were joined during forging, showed that the flow behaviour of the materials allowed secure locking and potential diffusion bonding during forging [18], [19],[20]]. In comparison to the other methods, forging of un-bonded preforms is less time consuming and more cost effective, since operations prior to forging are avoided.

1.4 Material Joining Challenges

1.4.1Metal Surfaces

The presence of contaminants and oxide layers on metal surfaces poses challenges to achieving successful metallurgical bonding in multi-metal forming processes. These

contaminants act as barriers to the formation of high-quality metallurgical bonds [21],[22]. Contamination layers such as grease, water, and oil vapor can be partially removed by using solvents or petrol. On the other hand, the oxide layer is much more challenging to remove completely since metal surfaces quickly become re-oxidized when in the presence of normal atmosphere [23]. The thickness and rate of oxide formation increase significantly at elevated temperatures.

The successful bonding of multi-metal components relies on the elimination of these contaminant and passivation layers. When the materials come into direct contact without these layers, interaction forces occur between the interfacial atoms, driven by cohesion forces at the surface of the materials. However, in a normal atmosphere, these cohesive forces are saturated by oxidation, hindering the formation of a strong metallurgical bond [23].

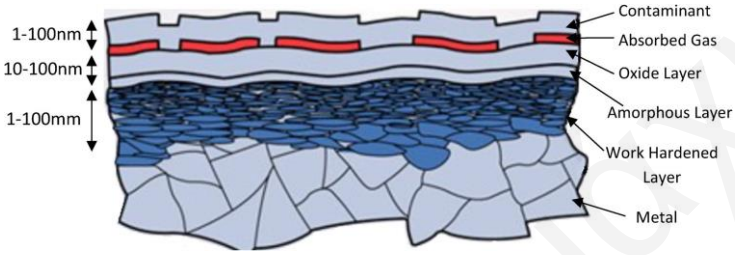

Figure 3: Contamination layers on a metal surface [24]

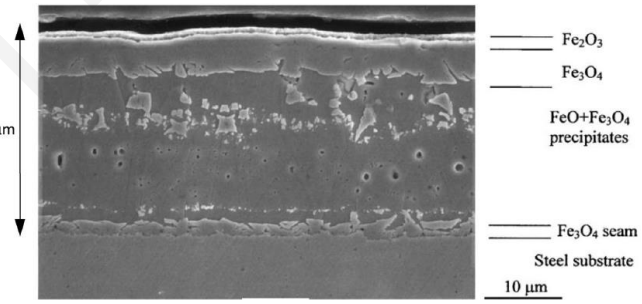

Figure 6: Formation of iron oxide on steel surface after heating in normal atmosphere [25]

1.4.2Intermetallic Layers

The bond strength between dissimilar metals is heavily influenced by the formation of brittle intermetallic compounds at the interface. In the bonding between steel and aluminum alloys, the formation of intermetallic compounds such as Al5Fe2 and Al2Fe may negatively affect the bond strength [26], [27], [28], [29]. Brittle intermetallic phases can lead to bond strengths that are 30% weaker than the strength of the weaker material [30].

The crystal structure of metals also affects adhesion [21], [23], with cubic structured metals such as iron or aluminum exhibiting higher adhesion compared to

hexagonal metals. Microstructural parameters such as the number of grains and orientation of crystallographic planes also influence adhesion properties.

1.4.3Galvanic Corrosion

Galvanic corrosion is a significant limitation in the direct bonding of dissimilar metals. It refers to the accelerated corrosion of a metal when in contact with another metal of higher potential [31]. The corrosion potential between dissimilar metals in contact determines the severity of galvanic corrosion, with the material with the lowest potential acting as the anode, while the material with the highest potential acts as the cathode.

To mitigate galvanic corrosion effects, spacer materials that are less susceptible to corrosion can be used as interlayer materials. These spacer materials help prevent direct contact between dissimilar metals and reduce the galvanic corrosion potential.

1.5 Strengthening the Intermetallic Bond

1.5.1Beneficial Conditions of Forging

Forging conditions can be beneficial for the formation of strong intermetallic bonds. Several factors contribute to this, including high temperature, pressure, relative material sliding, and time in contact. High temperature promotes adhesion and diffusion in the joint, as well as higher surface energy, resulting in accelerated diffusion of electrons and atoms across the bond [32]. Elevated temperatures also increase the ductility of the material, aiding in the breakup of passivation layers. Elevated pressures are known to promote solid-state welding [33], whereas relative sliding between the two materials has also been proven to be beneficial for solid-state welding processes.

In order to maximize metal-to-metal contact, disruption of the oxide layers is required to promote bonding. This can be achieved through the application of high

pressure, relative sliding, and other techniques that enhance the contact between the mating surfaces.

During forging, the plastic deformation that takes place, subjects the workpiece to high strains, which serve to disrupt surface oxide layers and expose clean metal layers, while simultaneously increasing the true contact area between the mating surfaces, as well as creating solid-state atomic bonds between the two contacting bulk metals.

The oxide layer itself is not eliminated or dissolved [34], but instead, it is fragmented and broken up to allow the parent metal to deform and flow around it. Therefore, macroscopic plastic deformation alone is not sufficient to achieve an ideal metallic bond. Microscopic plastic deformation operates on a similar principle, where the surface oxide layer is disrupted by the deformation of the microscopic asperities [35], [36]. In this case, increased surface roughness enhances the metallic contact between the surfaces and promotes subsequent metallurgical bonding. Therefore, when combined with macroscopic deformation, the use of high plastic strains and surface roughness has been shown to effectively promote intermetallic bonding.

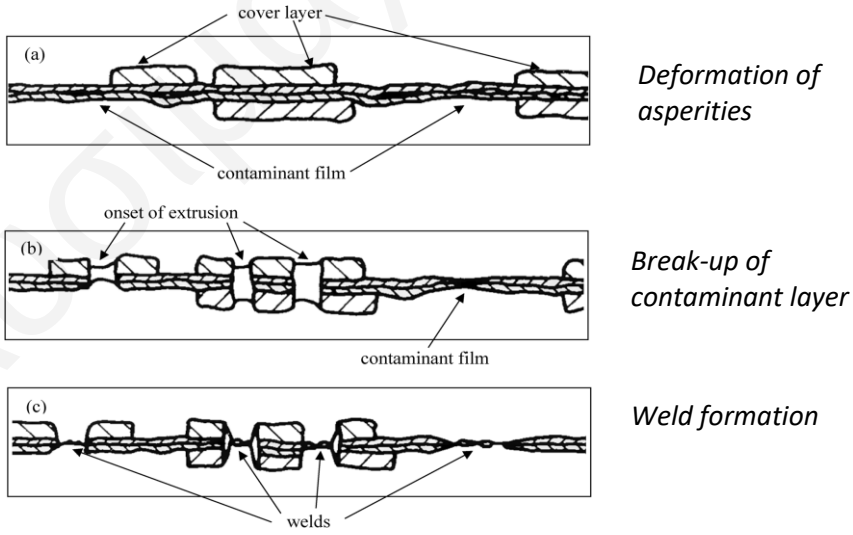

Figure 13: Solid state welding process [37]

1.5.2Interlayer Materials

The use of a third interlayer material has been proposed to promote bonding between dissimilar base metals [38], in order to address challenges such as galvanic

corrosion, that was mentioned previously, and differences in thermal expansion coefficient [39]. There are various interlayer materials and application methods suggested in the literature. One promising solution involves the use of a foil interlayer, where the deformation and splitting of the foil effectively remove oxide films from the contact area [40]. Copper foil and silver foil have been applied to the interface of aluminum and steel workpieces [41], while the application of brittle materials like nickel or chrome to the mating surfaces prior to solid-state welding can also promote the cracking of contaminants and passivation layers, exposing clean metal surfaces for better bonding.

Additive manufacturing technologies offer another avenue for applied interlayer materials. It has been proposed to additively manufacture an outer layer or coating, which could potentially be extended to interlayer applications [11]. Studies have primarily focused on using a solid inner material with an additively manufactured powder outer layer [42], [43]]. This method would benefit workpieces with high oxidizing potential, such as steels, to prevent the formation of an oxide layer in the interface during subsequent forging.

Chapter 2

2 EXEPRIMENTAL PROCEDURES AND RESULTS

2.1 Forging of Gears

2.1.1Experimental Setup

Hydraulic Press

The main piece of the experimental setup, the YQ41-100 C-frame, single-arm body hydraulic press of 100 tf capacity, shown in *Figure 6*, holds both the toolset and the sensors for data collection. Its working table dimensions are 700mm x 500mm and its pressing speed is 8 mm/s. The maximum Opening Height of the hydraulic press is 700 mm, while the Ram Stroke is 320 mm, meaning that the minimum Closing Height is 380 mm. The movement of the slide is controlled with integrated buttons, while the hydraulic press is also equipped with light curtains (*Figure 7*), for safety purposes. A beam of light is transmitted from the transmitter to the receiver, and if the light curtain is broken, the press will not actuate, and any downward movement of the press stops. Moreover, fixed safety guards made from a metal-mesh material surround the sides of the press to ensure physical guarding. Additional information and performance characteristics can be found in Appendix A.

Figure 6: Hydraulic Press

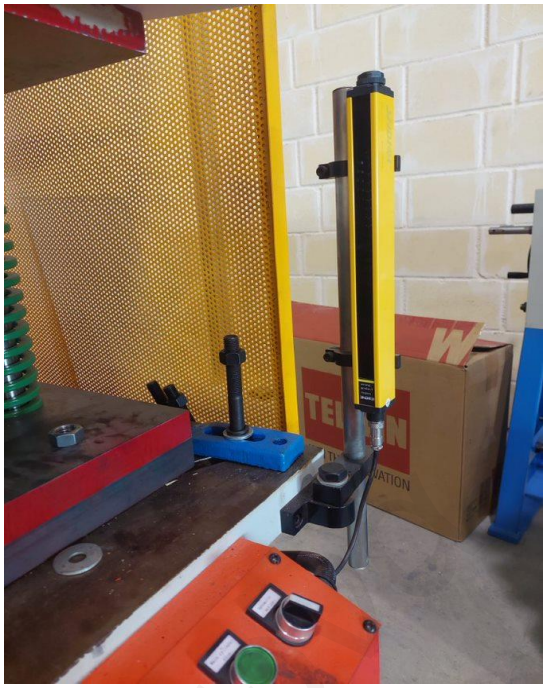

Figure 20: Light curtain installed on the hydraulic press

Basic and forging toolset

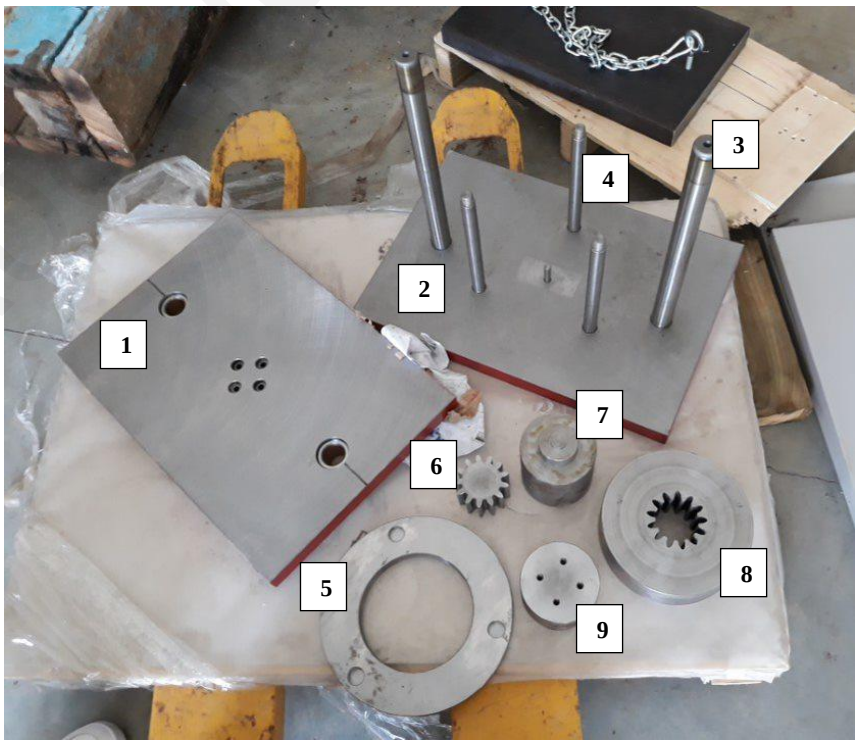

Figure 32: Disassembled toolset

Table 1: Name of parts pictured in Figure 8

No. of part (*Figure 8*)	Part name
1	Top plate
2	Bottom plate
3	Basic toolset guide pillar (taller pillar)
4	Forging toolset guide pillar (shorter pillar)
5	Ring
6	Counterpunch
7	Alignment tool
8	Die
9	Punch

The basic toolset, 'Eco-Line' Steel Die Set without Stripper from Fibro, consists of a base and top plate connected with two press fitted guide pillars. Around each pillar a Fibro high performance compression spring was placed. Details of model names are presented in *Appendix B*. The forging toolset was designed and manufactured in Cyprus and was made of mild steel $(E = 200\ GPa, \sigma_y = 250\ MPa,\ \sigma_{ut} = 400 - 550\ MPa)$. It is comprised of a punch mounted on the top plate and secured with four fasteners, a closed die (*Figure 9*) on springs, a gear shaped counterpunch (*Figure 10*) and an alignment tool responsible for keeping the counterpunch centered. The aim is the manufacturing of a $13 - teeth$ and $5\ mm$ module spur gear of $75\ mm$ outer diameter. Additional details regarding dimensions and engineering drawings of the forging toolset can be found in *Appendix C*.

Figure 9: Closed die

Figure 33: Gear-shaped counterpunch

The assembly of both the basic and forging toolset takes place in several steps. Firstly, the base plate is positioned on the working table of the hydraulic press. Besides the two guide pillars, three smaller pillars, with the appropriate Fibro springs, are secured on the base plate, as pictured in *Figure 11*, that hold a ring on which the die is positioned. In the center of the base plate, a metallic pin protrudes (*Figure 11*) in order for the alignment tool to be placed correctly every time. A hole at the bottom of the alignment tool matches the extruded pin, allowing the right positioning. Then, the top plate is secured with guide bushes on top of the two guide pillars, as demonstrated in *Figure 12*. At that point, the forging toolset can be assembled. The alignment tool is placed first, followed by the ring that passes through the three smaller guide pillars (*Figure 13*). Next, the die is situated on the ring and the gear-shaped counterpunch is fitted through the die and secured on the alignment tool (*Figure 14*).

Figure 35: Base plate with two basic toolset guide pillars with springs, three forging toolset guide pillars and pin in the centre for alignment

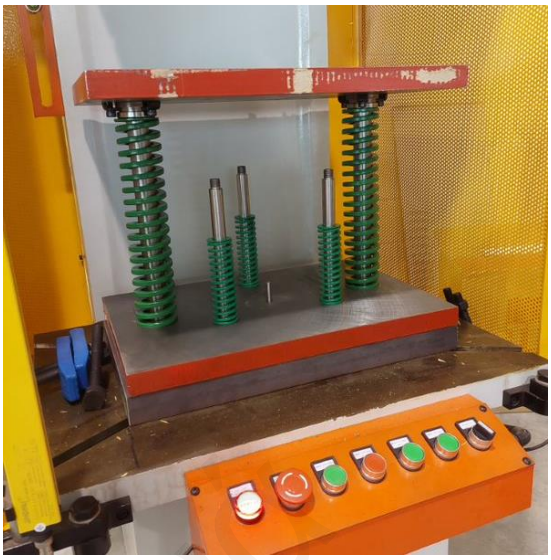

Figure 35: The top plate is secured on the guide pillars with two guide bushes

Figure 43: Placement of alignment tool and first ring through the smaller pillars

Figure 45: Placement of die on top of the ring

Figure 53: The second ring is placed on top of the die

Figure 53: The punch is fastened at the downside of the top plate

Another ring is fitted through the three smaller pillars and lays on top of the die, as shown in *Figure 15*. The smaller pillars have a threaded top part, thus permitting the securing of the ring with a nut on each pillar. Finally, as pictured in *Figure 16*, the punch is fastened at the downside of the top plate.

Sensors

Two sensors, one for measuring applied force and one for measuring the top plate's distance, are installed on the hydraulic press. The LCM Systems CDIT-1 Load Cell is positioned above the top plate (*Figure 17*) and measures the applied force from the hydraulic press in units of ton-force. The Load Cell is connected to a DSCUSB Load Cell adapter (*Figure 18*), which connects to a computer via USB cable. A software called DSCUSB Toolkit from LCM Systems needs to be installed on the computer, in order to have real-time indication of force value and data logging of force versus time to a .csv file. The log interval was chosen to be $100\ ms$, to satisfy the data recording based on the pressing speed.

Figure 55: The Load Cell is placed on the top plate

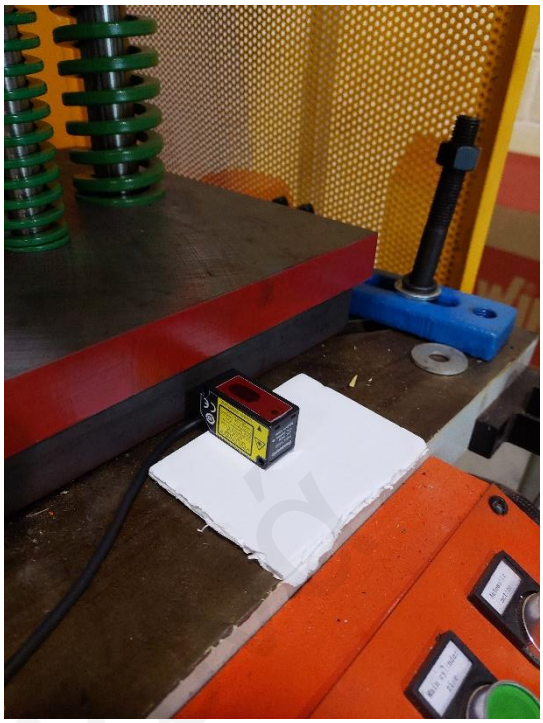

Figure 55: The Laser Distance Sensor is placed on the bolster

The Panasonic Micro Laser Distance Sensor ME-HGC1000 (*Figure 18*) is positioned on the bolster so that it is emitting the laser beam towards the top plate. The appropriate positioning of the sensor was crucial, since it can only measure distance in the range of $200\ mm - 600\ mm$. Due to the high pressing speed, there was the need to automatically record the data and store it in a file where it could be edited later. Therefore, an Arduino UNO microcontroller board (*Figure 19*) was connected to both the Laser Distance Sensor and a computer and via the PuTTY app installed on the computer, a .txt file with the distance data could be produced. The sampling rate was chosen to be $100\ ms$, the same as the sampling rate of the Load Cell. The sampling rate can be altered from the Arduino sketch, that can be found in *Appendix D*. Real-time indication of the distance values on the computer is also possible, through the Arduino software.

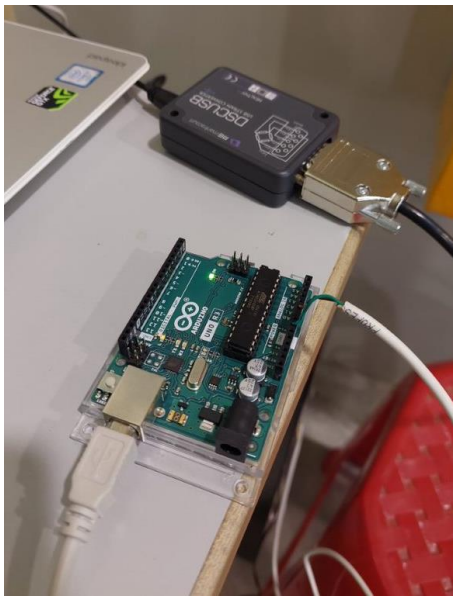

Figure 56: The Arduino Uno microcontroller and the DSCUSB Load Cell adapter

Furnaces

Two individual SNOL Muffle Furnaces 13/1100 LHM01 (Omron E5CC-T Controller) (*Figure 20*) are placed next to the hydraulic press at the lab. They are used for the simultaneous heating of the dissimilar metal samples, prior to them being placed inside the die and forged.

Figure 57: The two SNOL Muffle Furnaces

Metal Samples

For each experiment two un-bonded pieces were used, an outer ring and an inner cylinder, as seen in *Figure 21* and *Figure 22*. The outer rings were made of S235 steel, and the inner cores were made of AA6062 aluminium. The rings used were either of thickness of 1 mm or 3 mm, while the inner cylinders were of diameter of 46 mm or 42 mm, respectively. A set of experiments were also carried out using 3 mm outer rings made of AA6062 aluminium and 42 mm diameter inner cylinders made of AA2007. All the aluminium samples used during the experiments were annealed prior to forging, in order to achieve the greater deformation possible. The material combinations and the dimensions of the metal samples are summarized in *Table 2*. Additional details regarding the annealing process are discussed in the following section.

Table 2: Material combinations and dimensions of outer rings and respective inner cylinders

Outer ring			Inner cylinder		
Material	**Ring thickness**	**Height**	**Material**	**Diameter**	**Height**
S235	**3 mm**	37 mm	AA6062	Ø42 mm	40 mm
S235	**1 mm**	37 mm	AA6062	Ø46 mm	40 mm
AA6062	**3 mm**	37 mm	AA2007	Ø42 mm	40 mm

Figure 59: Un-bonded steel outer ring and aluminium inner cylinder

Figure 59: Assembled steel ring and aluminium cylinder

In certain experiments, a thin film of either copper (*Figure 23*) or silver (*Figure 24*) of 0.1 mm thickness, was positioned on the outer ring and inner core interface, in order

to enhance their bond. Mechanical properties of the materials used in the experiments are presented in the following table.

Table 3: Mechanical properties of materials used in the experiments

Material	Young's Modulus [GPa]	Yield Strength [MPa]	Ultimate Tensile Strength [MPa]
S235	210	235	360
AA6062	70	270	330
AA2007	71	250	390
Copper	110	33.3	210
Silver	76	54	110

Figure 61: Rectangular piece of copper film

Figure 61: Rectangular piece of silver film

Prior to forging, the aluminium cylindrical samples were also sanded with 80 Grit Sandpaper to create a rough outer surface, as seen in *Figure 25* and *Figure 26*. The increased roughness targets to enhance the material interlocking between the outer ring and the inner cylinder.

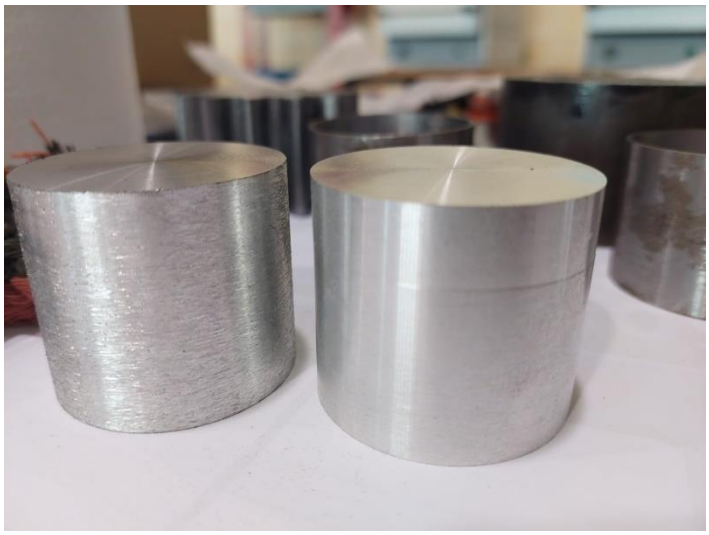

Figure 63: Comparison of sanded part (left) and non-sanded part (right)

Figure 63: Surface of sanded aluminium

Safety equipment

For safety reasons, it was required to wear a lab coat and safety glasses throughout the experiments. For the handling of the samples, both when placed inside the SNOL Muffle furnaces and when they were finally heated and removed to be positioned inside the die, additional equipment was needed. The Pro Mini Mouth Graphite Crucible 13" Tongs (*Figure 27*) from Tools and Tools UK were used for the transportation of the samples, while heat resistant gloves (*Figure 28*) were worn when approaching the hot furnaces. Working gloves were also used when lubricating the toolset and afterwards when the forged part was removed from the die, in order to avoid coming in direct contact with the applied grease.

Figure 65: The Pro Mini Mouth tongs

Figure 65: Heat resistant gloves

2.1.2Annealing of aluminium samples

As mentioned, all the aluminium samples were annealed before the experiments. That was the result of two test experiments which were conducted to determine if annealing was necessary. One non-annealed and one annealed aluminium cylinder of the same diameter, were forged, after both of them were heated for 15 minutes to 500 °C. The maximum force applied to the non-annealed cylinder was $93.6\ tf$, while the maximum force applied to the annealed cylinder was $92.7\ tf$, as observed in *Plots 1 and 2*.

Plot 1: Force vs Time of forged Non-annealed aluminium sample

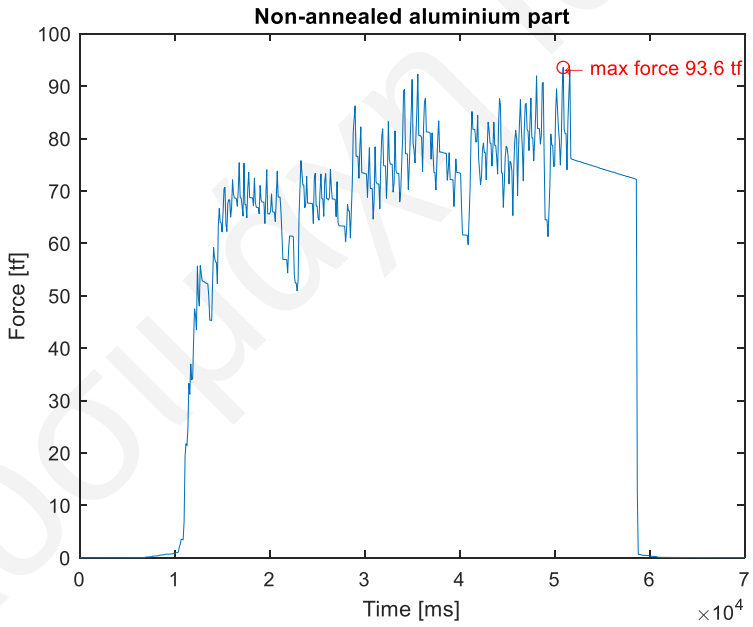

Plot 2: Force vs Time of Annealed forged aluminium sample

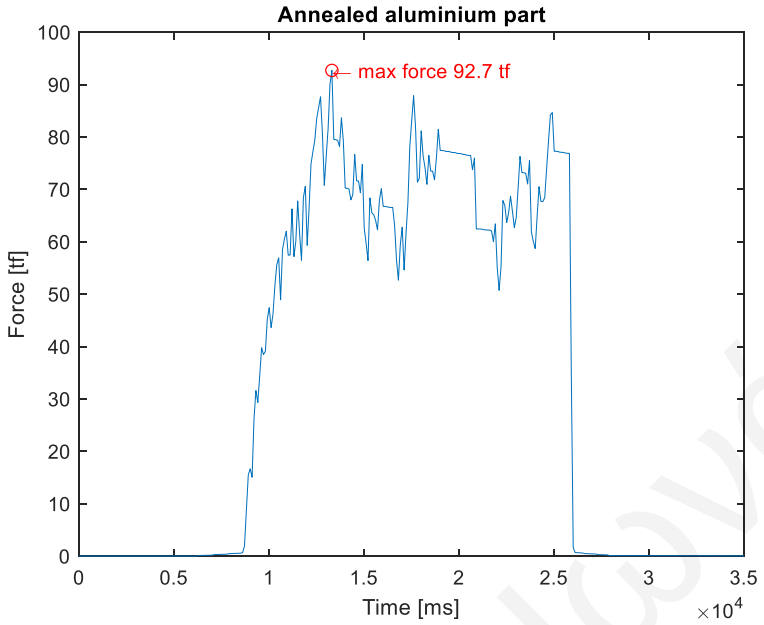

Despite the fact that the height of the non-annealed cylinder was smaller than the height of the annealed one, the maximum force applied was almost the same, but the deformation achieved was significantly less. As seen in *Figure 29*, *Figure 30* and *Figure 31*, the annealed cylinder was largely deformed and resembled a gear shaped item, whereas the non-annealed changed shape only slightly.

Figure 29: Side view of forged annealed (left) and non-annealed (right) aluminium parts

Figure 30: Forged annealed aluminium part

Figure 31: Forged non-annealed aluminium part

For the annealing of the samples, they were placed inside one of the SNOL furnaces and were heated to approximately 410 °C for 3 hours. Then, they were cooled by 20 °C per hour until reaching 290 °C. When 290 °C were achieved, the furnace was switched off.

2.1.3Experimental Process

The experimental procedure is done in multiple stages, before achieving the forged part. The required actions are as follows:

Heating of samples:

- The samples, both the outer ring and the inner cylinder, are cleaned with acetone in order to remove any contaminants on their surface that would prevent the formation of the metallurgical bond.

- Then, the outer ring is placed in SNOL furnace A and the inner core in SNOL furnace B and are heated for 15 minutes. If the outer ring is steel, then it is heated to 950 °C, whereas if it is made of aluminium is heated to 550 °C. Since the inner cylindrical samples are all of aluminium, they are always heated to 550 °C. For the experiments where a film is applied, the film is cut in a rectangular shape of appropriate dimensions so it can be wrapped around the inner surface area of the ring (*Figure 32*). Then, the ring with the film is placed inside the furnace to be heated.

Lubrication:

- Before each forging process, Omega 35 (*Figure 33*), a high temperature grease, is applied with a brush on the punch, the die and the counterpunch.

Figure 32: Copper film wrapped on the inside surface of the AA6062 ring

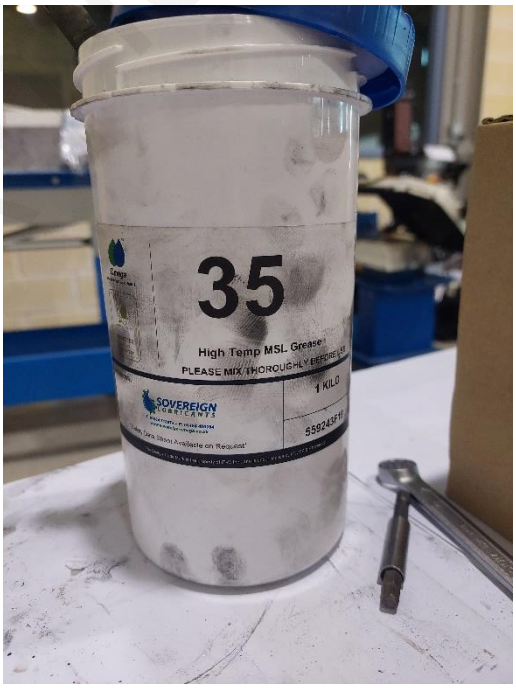

Figure 33: The Omega 35 high temperature grease that was applied on the toolset

Data collection:

- The recording and storage of force and distance data, from the Load Cell and the Laser Distance Sensor respectively, is activated before the end of the 15 minutes of heating the samples.

Forging:

- Once the 15 minutes of heating are over, firstly the outer ring is removed with tongs from the SNOL furnace A and placed inside the die. Then, the inner core is removed with tongs from the SNOL furnace B and placed inside the outer ring.
- Next, the parts are compressed by the hydraulic press.

Removal of formed part:

- Due to the formation of flash (*Figure 34* and *Figure 35*), the forged part, the die and the counterpunch are joined together. Thus, they must be removed together, after the punch is uninstalled from the toolset.
- Afterwards, the joined parts (*Figure 36*) are transported to a manual 50 ton-force press (*Figure 37*), in order to eject the forged part.

Figure 34: The forged part and counterpunch are joined due to flash

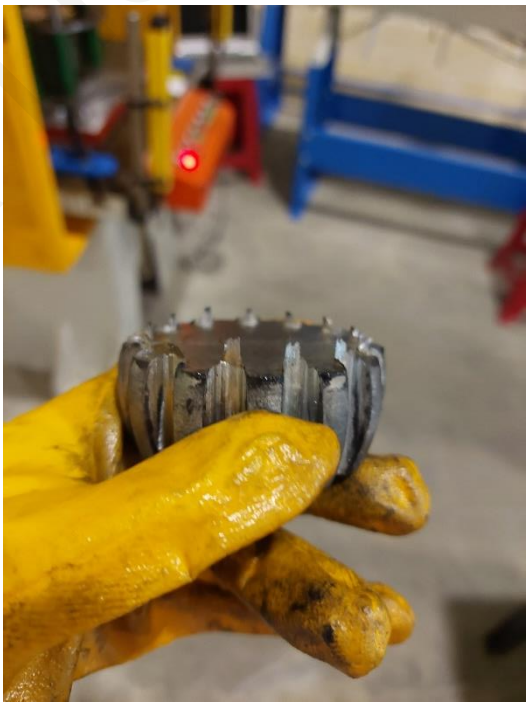

Figure 35: Flash formed on the forged part

Figure 36: Removal of joined part, die and counterpunch

Figure 37: Positioning of joined parts in the manual press

Removal of oxides from the toolset:

- After the parts are separated, a wire brush is used to clean the die (*Figure 38*), the punch, and the counterpunch (*Figure 39*) from remaining oxide flakes. The residual oxides were developed on the outer ring and the inner core due to heating inside the furnaces.

Figure 38: Oxide residues on the die

Figure 39: Oxide flakes on the counterpunch

2.1.4 Results

In total, nine experiments were conducted using the different metal combinations, as seen in *Table 4*. As mentioned previously, all the aluminium samples were annealed before they were forged. Some of the experiments were carried out twice, whereas the others due to challenges mentioned in the following pages were conducted only once. In *Table 4*, the experiments are presented in chronological order, with the '*3 mm S235 ring - Ø42 mm AA6082 core*' experiment to be the first one that was conducted.

Table 4: Metal combinations used in the experiments in chronological order

Experiment	Metal combination
1	3 mm S235 ring - Ø42 mm AA6082 core
2	1 mm S235 ring - Ø46 mm AA6082 core
3	3 mm AA6082 ring - Ø42 mm AA2007 core
4	3 mm AA6082 ring - Ø42 mm AA2007 core – Cu film
5	3 mm AA6082 ring - Ø42 mm AA2007 core – Ag film
6	3 mm AA6082 ring - Ø42 mm AA2007 core **(2nd try)**
7	3 mm AA6082 ring - Ø42 mm AA2007 core – Cu film **(2nd try)**
8	3 mm AA6082 ring - Ø42 mm AA2007 core – Ag film **(2nd try)**
9	3 mm S235 ring - Ø42 mm AA6082 core – Ag film

For each experiment, the experimental process mentioned above was followed. The data obtained from the Load Cell and the Laser Distance Sensor were processed and plotted and in addition, the maximum force and distance value was noted for each experimental try. The raw force and distance data were plotted versus time and are presented in *Appendix E*. Moreover, the processed force and distance data were plotted and are presented in comparison with a polynomial trendline, while the raw force vs distance plots with noise are in *Appendix E*. The noise originated from the non-constant force application when the punch was in contact with the metal samples and the die. For safety reasons, the slide's movement was controlled manually by pressing a button, thus resulting in a changing force application. As a result, both distance and force fluctuations can be noticed in the plots in *Appendix E*.

Experiment 1: 3 mm S235 ring - ∅42 mm AA6082 core

The first experiment conducted was the forging of an outer 3 mm S235 ring and an inner AA6082 core of 42 mm diameter. Although the maximum force applied reached the 83.73 tf, the deformation achieved was insignificant. As shown in *Figure 40*, it is clear that there is no teeth formation, only a slight deformation on the outer ring due to the die's shape.

Table 5: Experiment 1 maximum distance and force value, trendline equation and R-squared value

	Experiment 1
Maximum distance value [mm]	85
Maximum force value [tf]	83.73
Trendline equation	$y = 0.0186x^2 - 0.6572x + 3.146$
R-squared value	0.9804

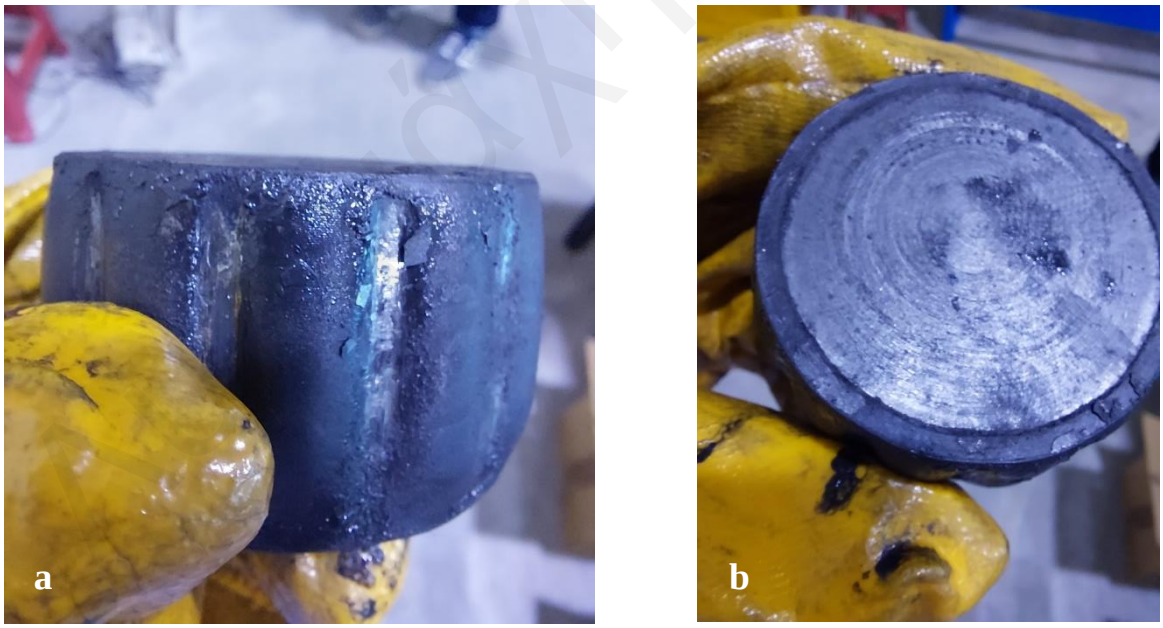

Figure 40: (a) Side view and (b) Top view of gear 1

Plot 3: Force vs Distance and Trendline for Experiment 1

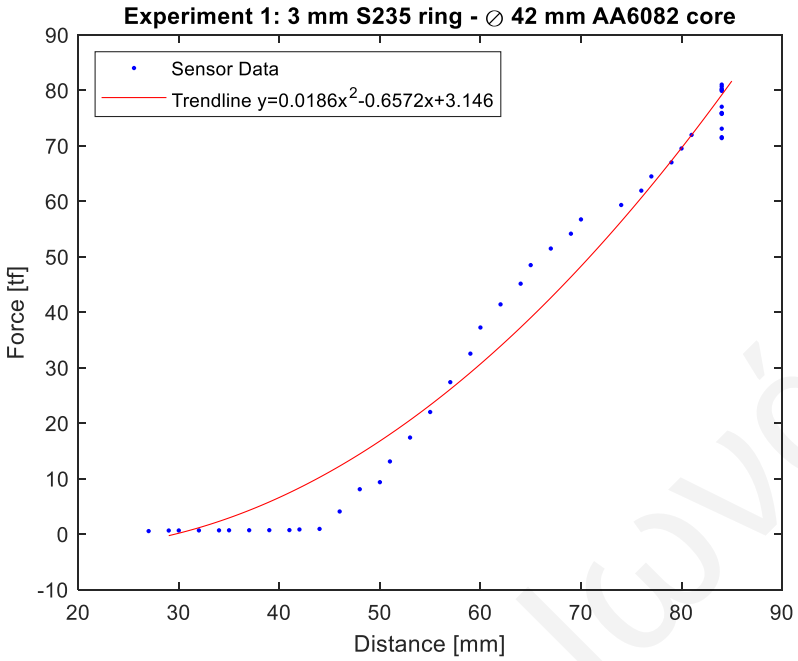

Experiment 2: 1 mm S235 ring - Ø46 mm AA6082 core

The next experiment was carried out with a 1 mm S235 ring and an inner AA6082 core of 46 mm diameter. A thinner size ring was chosen, in order to test whether a larger sample deformation could be achieved. With a maximum force of 89.64 tf, compared to the 83.73 tf of gear 1, and the same maximum distance of 85 mm, a more noticeable deformation was achieved. As seen in *Figure 41*, the gear teeth are shaped better, however they do not have a uniform shape. From *Figure 41*, it can also be seen that the outer ring has teared, resulting in separated pieces attached to the formed teeth. Also, it was noted that the steel pieces in some parts were falling off due to not being bonded with the inner aluminium core.

Table 6: Experiment 2 maximum distance and force value, trendline equation and R-squared value

	Experiment 2
Maximum distance value [mm]	85
Maximum force value [tf]	89.64
Trendline equation	$y = 0.0002x^3 - 0.0382x^2 + 2.861x + 0.1123$
R-squared value	0.9567

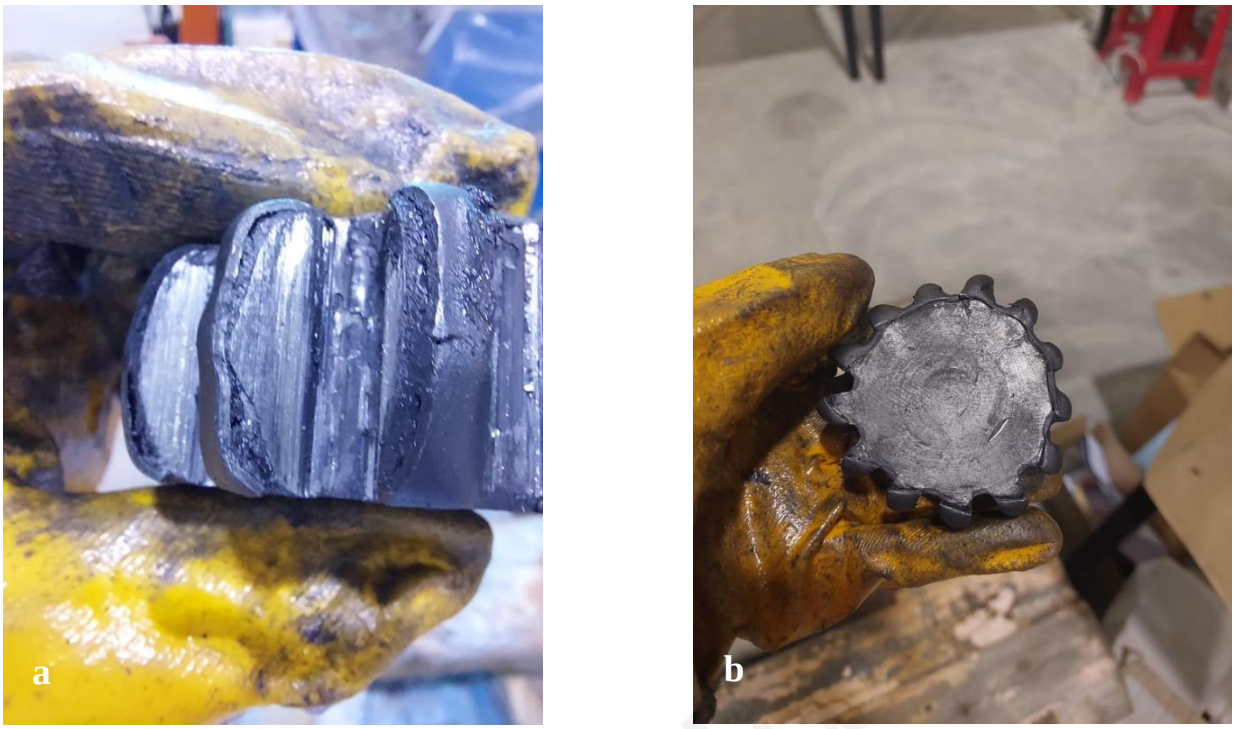

Figure 41: (a) Side view and (b) Top view of gear 2

Plot 4: Force vs Distance and Trendline for Experiment 2

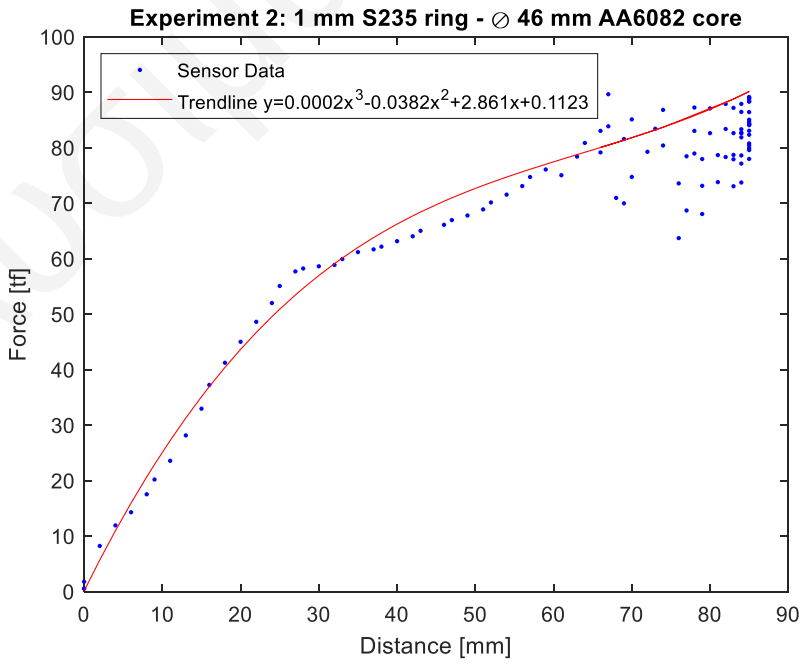

Experiment 3 and 6: 3 mm AA6082 ring - Ø42 mm AA2007 core

Since the experiments with steel as the outer material did not result in the desired gear shape, it was decided to test the AA6082 aluminium as the outer layer and the aluminium AA2007 as the inner material. Two experiments in total were conducted with this material combination. As seen from *Figure 42* and *Figure 43*, the shape of the gear teeth and the final height of the gears were very similar, although the maximum force and distance (*Table 7*) recorded for gear 6 were smaller compared to gear 3.

Table 7: Experiment 3 and 6 maximum distance and force value, trendline equation and R-squared value

	Experiment 3: 1st try
Maximum distance value [mm]	88
Maximum force value [tf]	86.35
Trendline equation	$y = 3 \cdot 10^{-5}x^4 - 0.0048x^3 + 0.2175x^2 - 2.8023x + 0.3283$
R-squared value	0.9672
	Experiment 6: 2nd try
Maximum distance value [mm]	86
Maximum force value [tf]	79.17
Trendline equation	$y = 1 \cdot 10^{-6}x^5 - 0.0003x^4 + 0.0181x^3 - 0.4962x^2 + 4.6854x - 5.3117$
R-squared value	0.9517

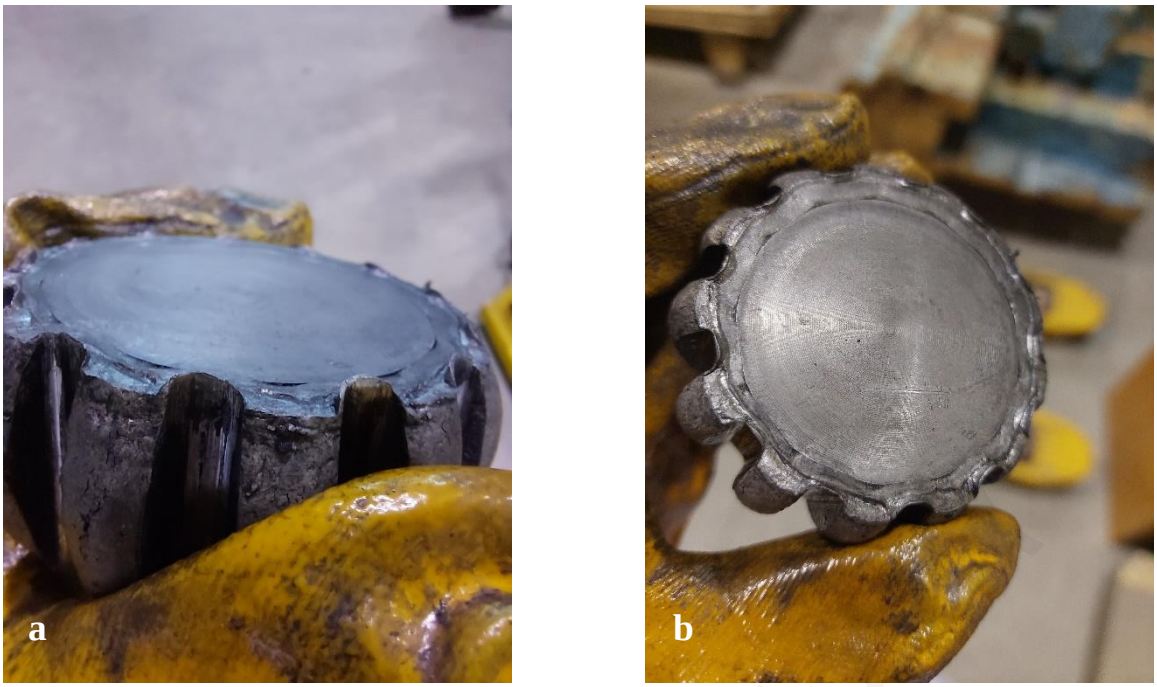

Figure 42: (a) Side view and (b) Top view of gear 3

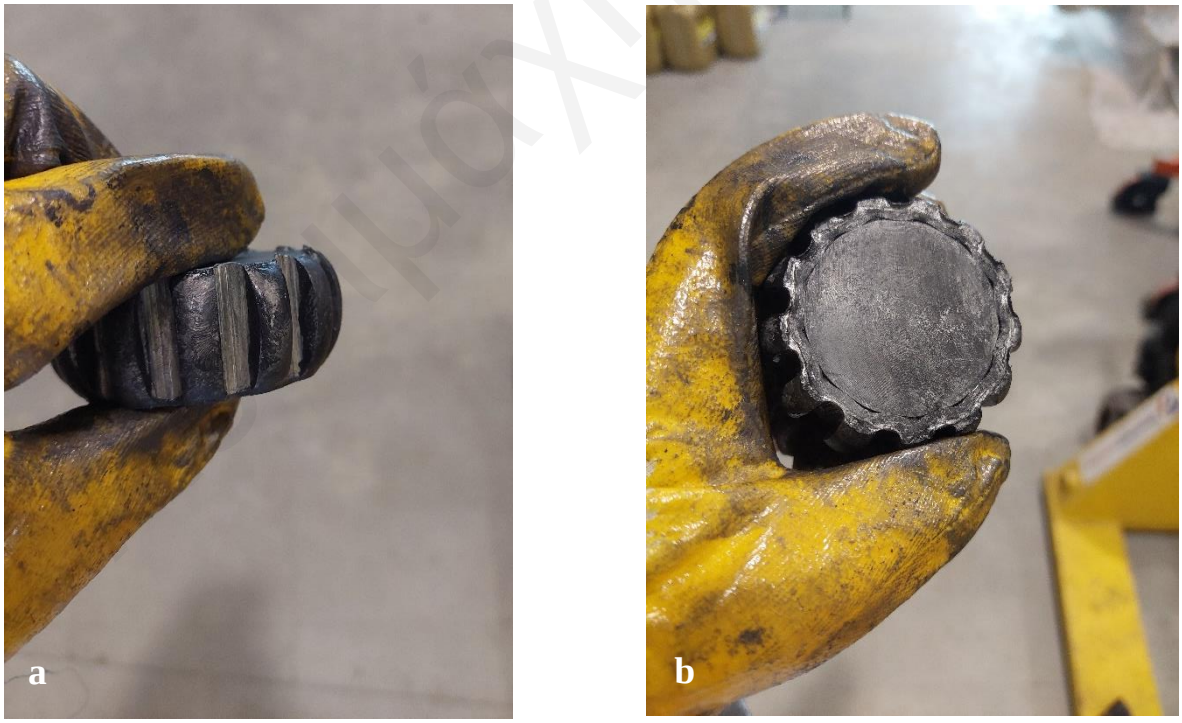

Figure 43: (a) Side view and (b) Top view of gear 6

Plot 5: Force vs Distance and Trendline for Experiment 3

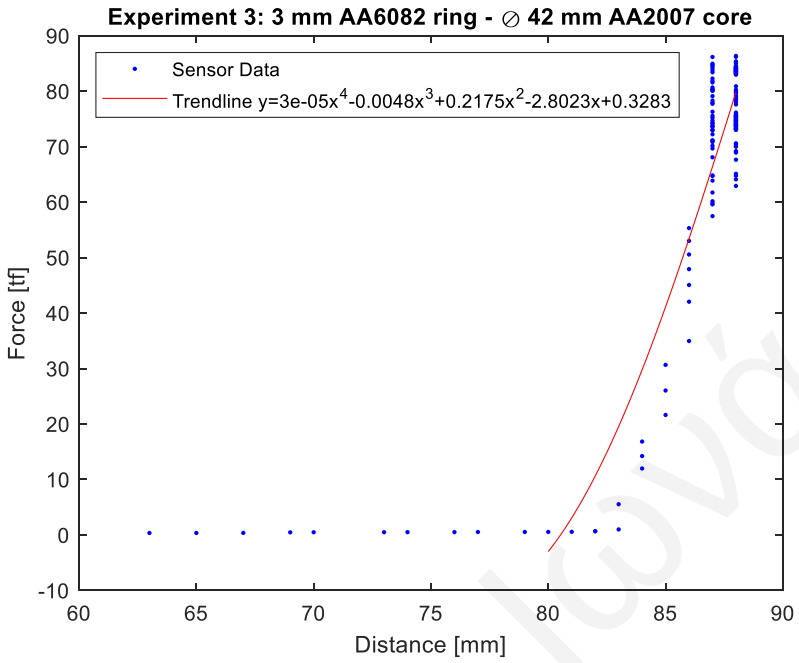

Plot 6: Force vs Distance and Trendline for Experiment 6

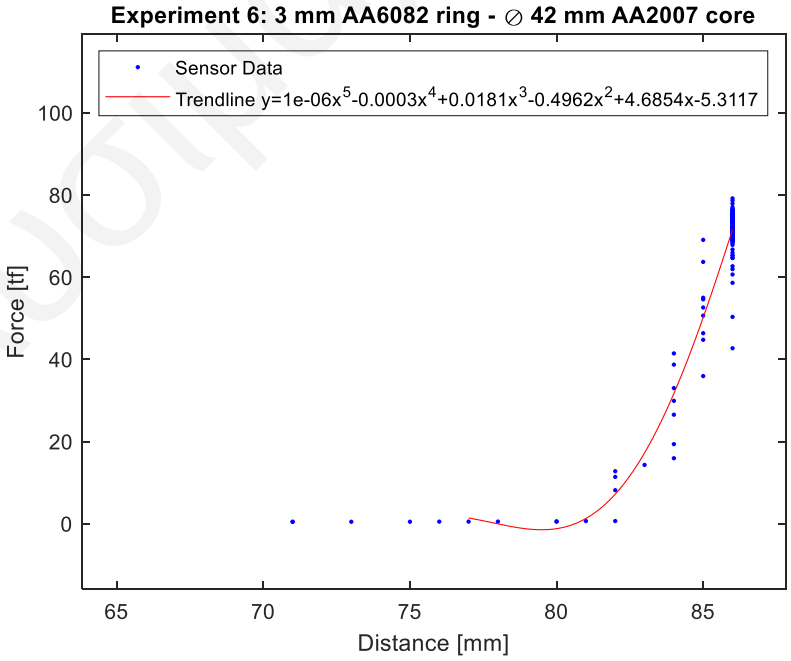

Experiment 4 and 7: 3 mm AA6082 ring - Ø42 mm AA2007 core – Cu film

Another set of experiments were conducted with aluminium materials, with the only difference that a copper film was wrapped on the inside surface of the outer ring prior to heating and forging, in order to test if the film will enhance the intermetallic bond. In both experiments the maximum distance was the same, whereas the maximum force recorded was approximately 6 tf greater for gear 4 compared to gear 7 (*Table 8*). Again, even though the maximum recorded force was less for gear 7, it was slightly more deformed than gear 4.

Table 8: Experiment 4 and 7 maximum distance and force value, trendline equation and R-squared value

	Experiment 4: 1st try
Maximum distance value [mm]	81
Maximum force value [tf]	71.89
Trendline equation	$y = 0.0008x^3 - 0.0786x^2 + 1.9509x - 9.0765$
R-squared value	0.9821
	Experiment 7: 2nd try
Maximum distance value [mm]	81
Maximum force value [tf]	65.86
Trendline equation	$y = 1 \cdot 10^{-6}x^5 - 0.0002x^4 + 0.0149x^3 - 0.361x^2 + 2.8029x - 0.5741$
R-squared value	0.9175

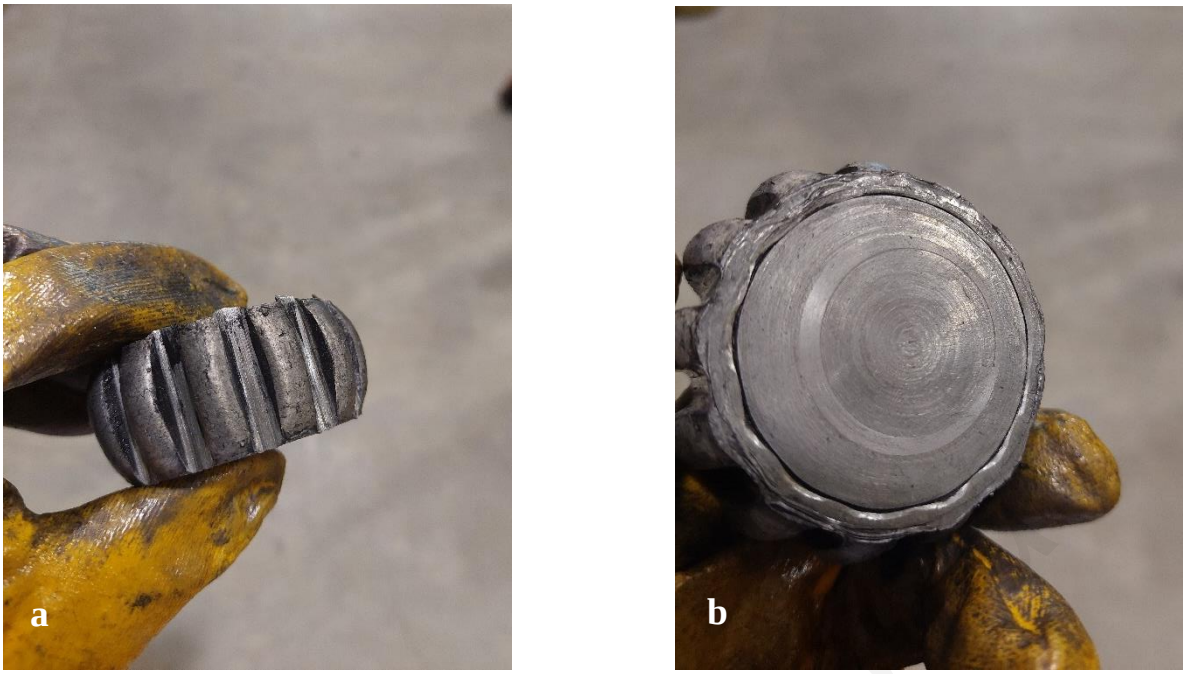

Figure 44: (a) Side view and (b) Top view of gear 4

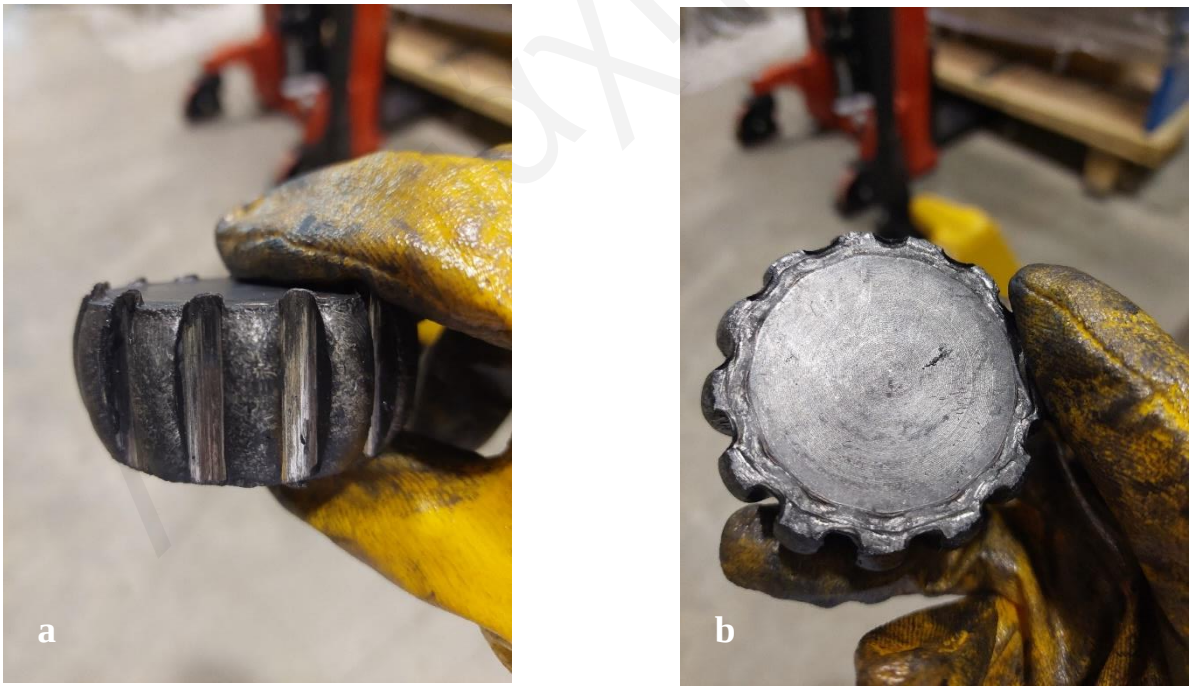

Figure 45: (a) Side view and (b) Top view of gear 7

Plot 7: Force vs Distance and Trendline for Experiment 4

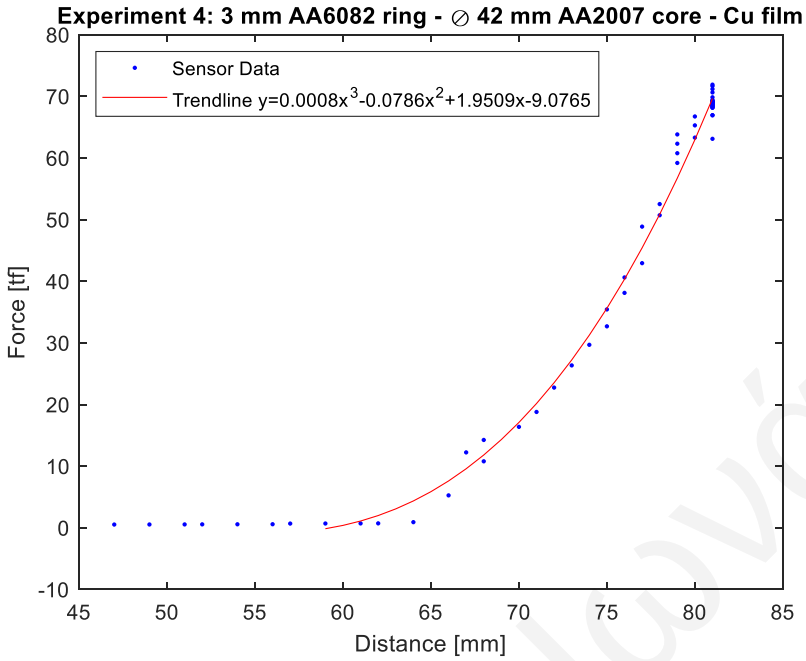

Plot 8: Force vs Distance and Trendline for Experiment 4

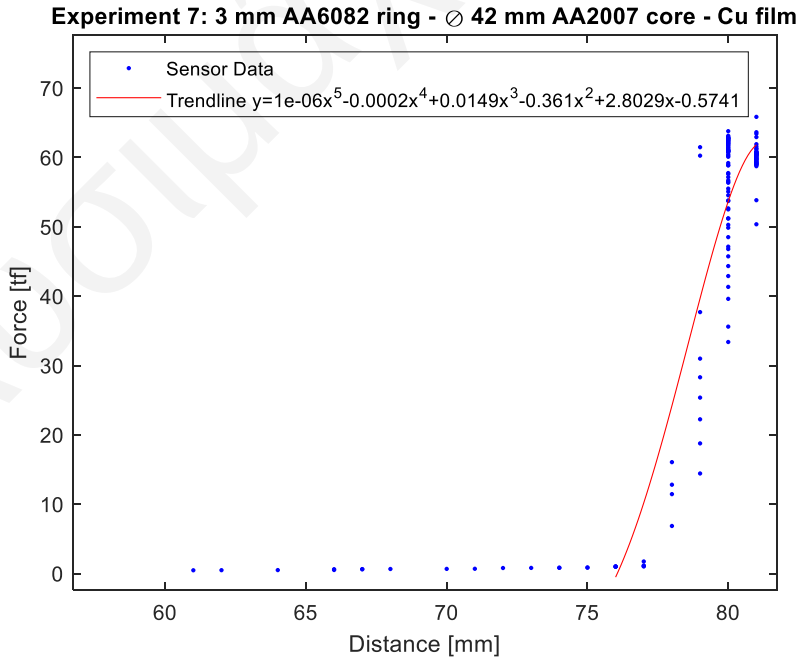

Experiment 5 and 8: 3 mm AA6082 ring - Ø42 mm AA2007 core – Ag film

Besides the copper film, a silver film was also tested. It was noticed that during heating the copper film was oxidized, so another film was put to test that did not show that behaviour. From the sensor data recorded, the maximum distance is approximately the same, while a huge difference in the maximum force applied is noticed (*Table 9*). The largest force recorded in all experiments was for the forging of gear 5, although that might be a result of the silver film displacement during the assembly inside the die. As shown in *Figure 46*, the silver film moved to the bottom of the outer ring and possibly pushed the aluminium core up, resulting in the compression of a smaller bi-metallic area. However, as seen in *Figure 46* and *Figure 47*, the teeth shape and final gear height seem very similar, with gear 8 being slightly more deformed.

Table 9: Experiment 5 and 8 maximum distance and force value, trendline equation and R-squared value

	Experiment 5: 1st try
Maximum distance value [mm]	85
Maximum force value [tf]	96.39
Trendline equation	$y = 0.026x^2 - 1.2168x + 5.1814$
R-squared value	0.9747
	Experiment 8: 2nd try
Maximum distance value [mm]	86
Maximum force value [tf]	74.48
Trendline equation	$y = 3 \cdot 10^{-5}x^4 - 0.0042x^3 + 0.1816x^2 - 2.2793x + 0.3362$
R-squared value	0.9550

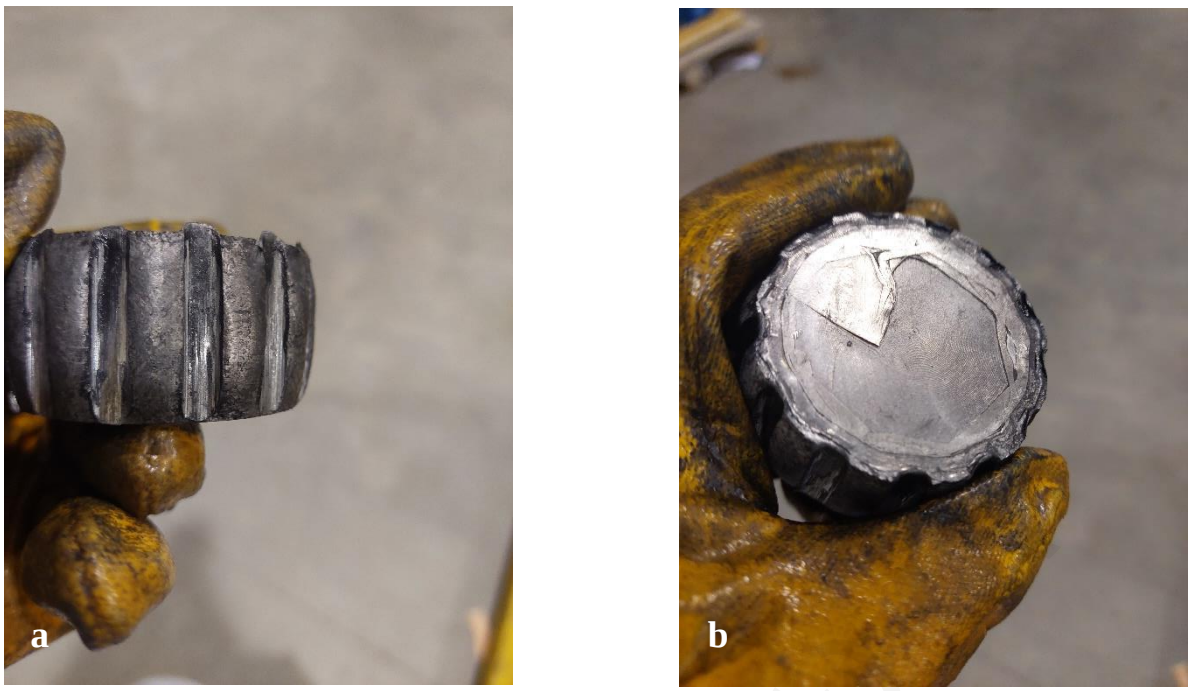

Figure 46: (a) Side view and (b) Top view of gear 5

Figure 47: (a) Side view and (b) Top view of gear 8

Plot 9: Force vs Distance and Trendline for Experiment 5

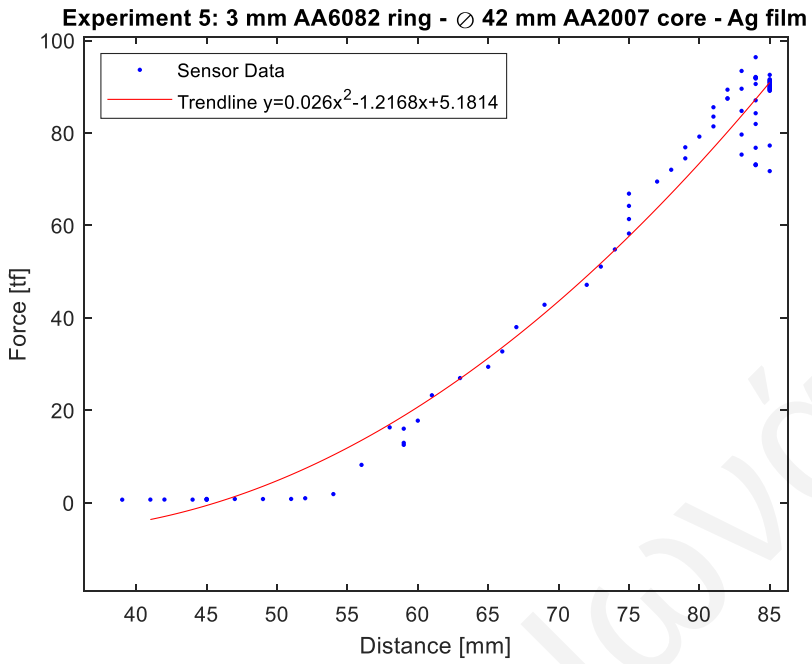

Plot 10: Force vs Distance and Trendline for Experiment 8

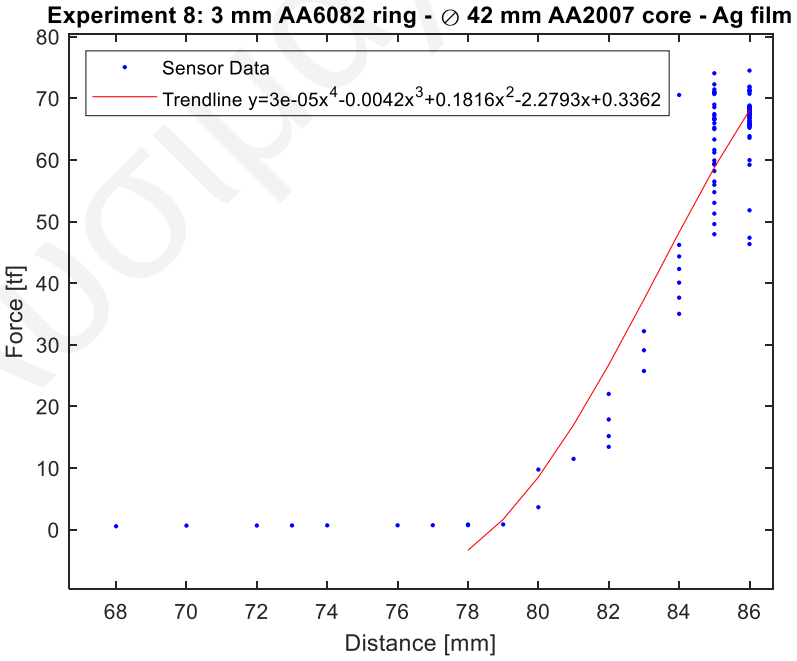

Experiment 9: 3 mm S235 ring - ∅42 mm AA6082 core – Ag film

The final experiment was conducted with 3 mm steel as the outer material and an inner AA6082 core of 42 mm diameter with a silver film applied in their interface. As expected from the first experiment, the deformation of the samples was not significant, as shown in *Figure 48*. The maximum distance recorded during the forging of gear 1 and 9 is approximately the same, while the maximum force for the formation of gear 9 was the lowest of all experiments (*Table 10*). However, the final height and diameter of gear 9 is almost identical to gear 1.

Table 10: Experiment 9 maximum distance and force value, trendline equation and R-squared value

	Experiment 9
Maximum distance value [mm]	84
Maximum force value [tf]	68.34
Trendline equation	$y = 0.0153x^2 - 0.594x + 0.568$
R-squared value	0.9771

Figure 48: (a) Side view and (b) Top view of gear 9

Plot 11: Force vs Distance and Trendline for Experiment 9

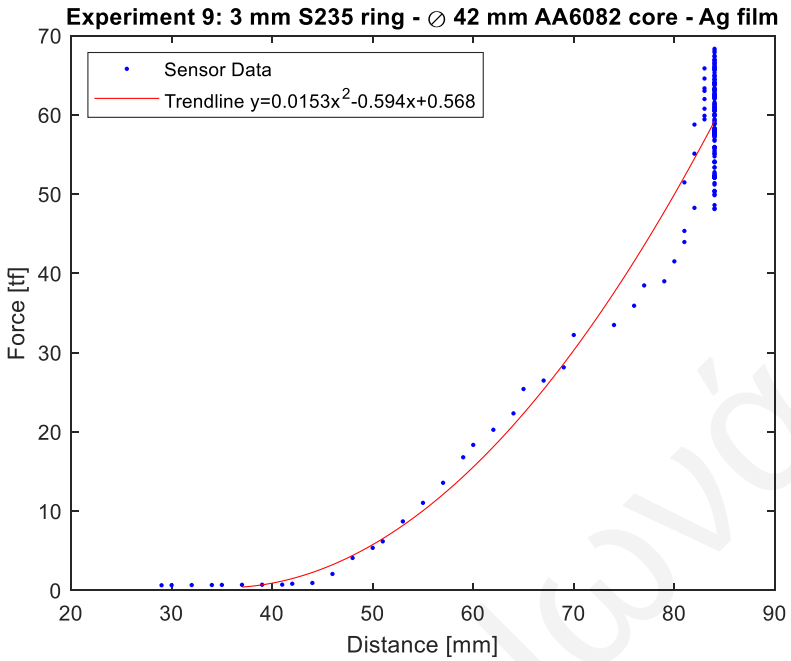

Table 11: Summary of maximum distance and force values for the different metal combinations

Experiment	Metal combination	Maximum distance value [mm]	Maximum force value [tf]
1	3 mm S235 ring - Ø42 mm AA6082 core	85	83.73
2	1 mm S235 ring - Ø46 mm AA6082 core	85	89.64
3	3 mm AA6082 ring - Ø42 mm AA2007 core	88	86.35
4	3 mm AA6082 ring - Ø42 mm AA2007 core – Cu film	81	71.89
5	3 mm AA6082 ring - Ø42 mm AA2007 core – Ag film	85	96.39
6	3 mm AA6082 ring - Ø42 mm AA2007 core **(2nd try)**	86	79.17
7	3 mm AA6082 ring - Ø42 mm AA2007 core – Cu film **(2nd try)**	81	65.86
8	3 mm AA6082 ring - Ø42 mm AA2007 core – Ag film **(2nd try)**	86	74.48
9	3 mm S235 ring - Ø42 mm AA6082 core – Ag film	84	68.34

2.2 Cutting of Gears

The gears produced are then cut in approximately 1 *cm* thick rectangular sections, in order to later observe the intermetallic bond with an optical microscope. A simple part (*Figure 49*) was created to hold the gears in place, with two metal plates, a threaded bolt, four nuts and two washers, so they could be cut by the Bemato Sawing machine (*Figure 50*). Prior to cutting the gears, an off-centre hole (*Figure 51*) was drilled in the gear with a manual Bemato Drilling machine (*Figure 52*), so the threaded bolt could pass through it. One gear from each material combination was cut. In the case of two gears with the same material combination, the gear with the largest deformation was chosen. The gears chosen to be cut can be seen in *Table 12*.

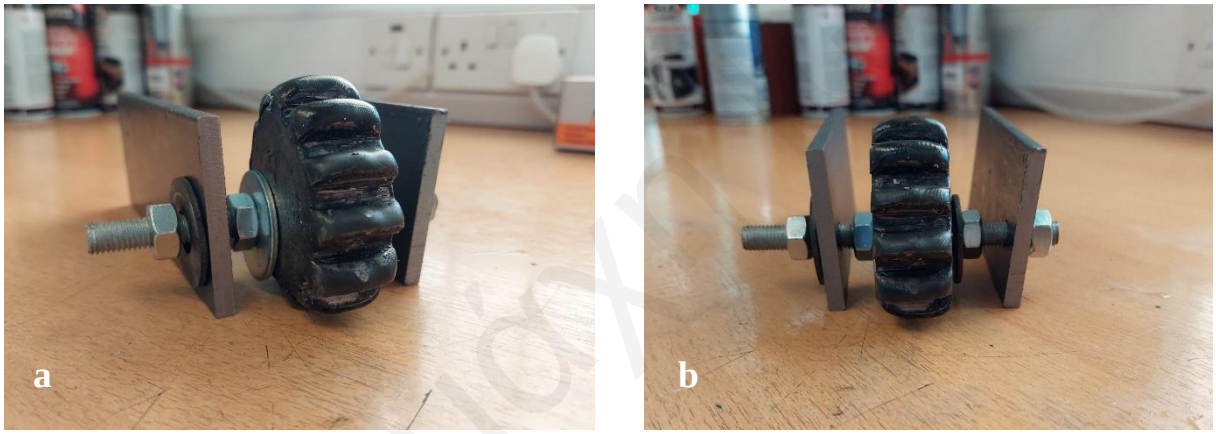

Figure 49: (a) Side view and (b) Front view of gear-holding part used for cutting the gears

Figure 50: The Bemato Sawing machine

Figure 51: Off-centred hole drilled on gear 2

Figure 52: The Bemato Drilling machine

The process of cutting gave an initial indication whether the different metals bonded during forging. The majority of the gears, as seen in *Table 12*, were unbonded, since the outer ring layer detached during cutting, as noted in the case for gear 1, shown in *Figure 53*, and gear 4, shown in *Figure 54*. Only the outer material layer on one side of both gears 2 and 8 remained intact after the cutting process, as seen in *Figure 55 and Figure 56*, respectively. Those rectangular sections were then polished, before they were observed under the microscope.

Table 12: Bonding results after cutting of gears

Experiment	Metal combination	Result
1	3 mm S235 ring - Ø42 mm AA6082 core	Un-bonded
2	1 mm S235 ring - Ø46 mm AA6082 core	**Bonded**
6	3 mm AA6082 ring - Ø42 mm AA2007 core **(2nd try)**	Un-bonded
7	3 mm AA6082 ring - Ø42 mm AA2007 core – Cu film **(2nd try)**	Un-bonded
8	3 mm AA6082 ring - Ø42 mm AA2007 core – Ag film **(2nd try)**	**Bonded**
9	3 mm S235 ring - Ø42 mm AA6082 core – Ag film	Un-bonded

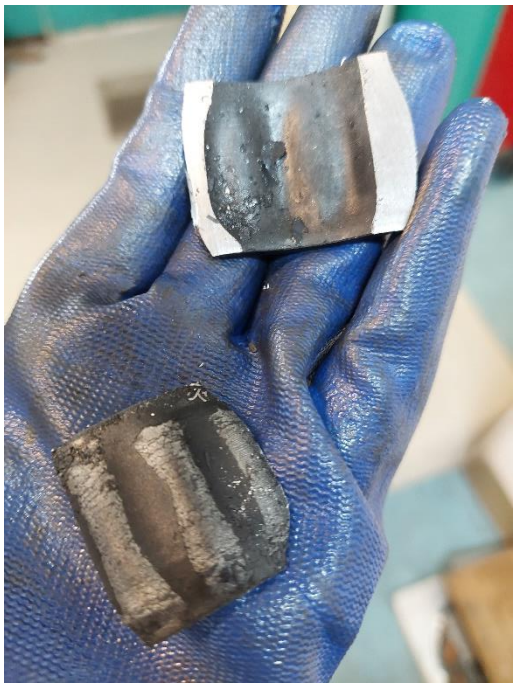

Figure 53: Detached pieces of gear 1, with oxide flakes observed on the outer layer

Figure 54: Detached outer layer of gear 4 with copper film

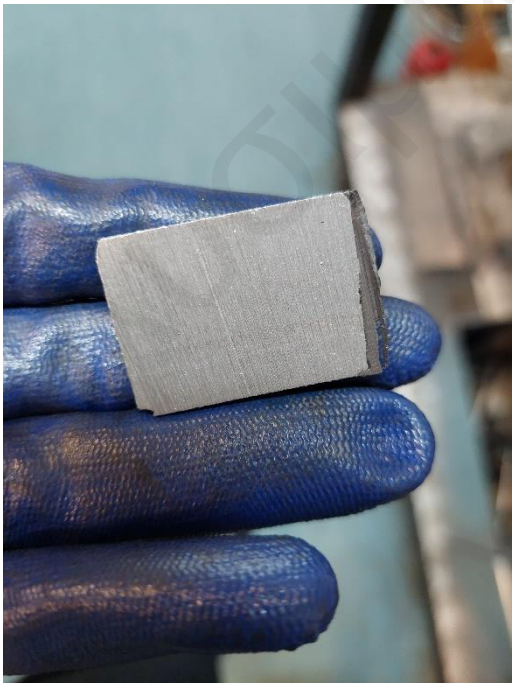

Figure 55: Rectangular section of gear 2

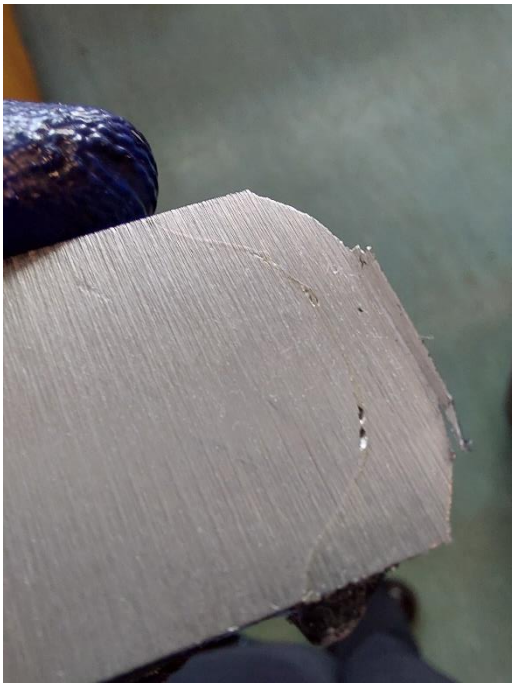

Figure 56: Rectangular section of gear 8

2.3 Polishing and Optical Microscopy

As discussed previously, the rectangular sections cut from the gears 2 and 8 were the only ones that remained bonded during the cutting process. Thus, those sections were firstly polished, so the interlayer between the outer and inner metal could be observed with an optical microscope.

Before the polishing process, a metallic cube was attached to the sections of gear 2 and 8 with wax, in order to have a better grip of the samples when polishing them. The cube was heated and then the wax was applied on its top surface, followed by the sample, as seen in *Figure 57*. After the cube cooled down and the wax hardened (*Figure 58*), different grinding papers with silicon carbide (SiC) particles were attached (*Figure 59*) on the Struers LaboPol 30 polishing machine (*Figure 60*), starting with the one with the biggest grain size. Then, a better finish is ensured by additional grinding using magnetic discs with cloth attached to them and special pastes with small particles.

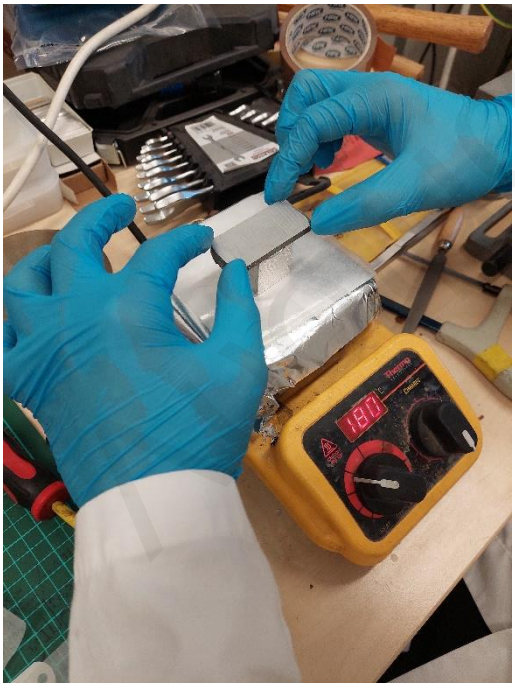

Figure 57: Heating of the metallic cube and securing the sample with wax

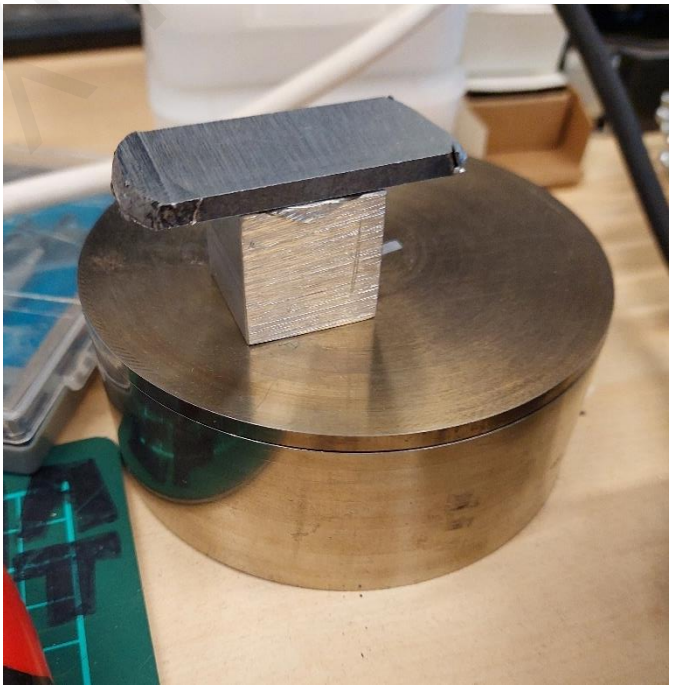

Figure 58: Waiting for the metallic to cool down and the wax to harden

Figure 59: Polishing of the sample

Figure 60: The Struers LaboPol 30 polishing machine

The order of disk use, in order to achieve the desired polishing result, is as follows:

- SiC Foil #P1000 – Grain size 18 μm
- SiC Foil #P2000 – Grain size 10 μm
- SiC Foil #P4000 – Grain size 5 μm
- Cloth disk with 3 μm paste
- Cloth disk with 1 μm paste

After the polishing was completed, the cube was heated again, the wax melted, and the polished sample could be removed. The surface of the sections of gear 2 and gear 8, resulted in a mirror effect, due to the polishing process. As seen in *Figure 61* and *Figure 62*, the polished section of gear 2 and gear 8, respectively, reflected the phone used to take the pictures.

Figure 61: The polished section of gear 2

Figure 62: The polished section of gear 8

The gap between the outer steel layer and the inner aluminium core of gear 2 is noticeable with the naked eye, as seen in *Figure 61*. However, in *Figure 62*, a slightly noticeable line can be detected between the outer aluminium layer and the inner aluminium core of gear 8, which in this case is the silver film.

The interface between the different metals was further observed in the Euromex Oxion Inverso optical microscope, seen in *Figure 63*. The microscope was connected to a computer (*Figure 64*), so high resolution images of the interfaces of gears 2 and 8 could be obtained. The samples were placed with the polished side facing down, on a specific spot on the microscope (*Figure 65*).

Figure 63: The Oxion Inverso optical microscope from Euromex

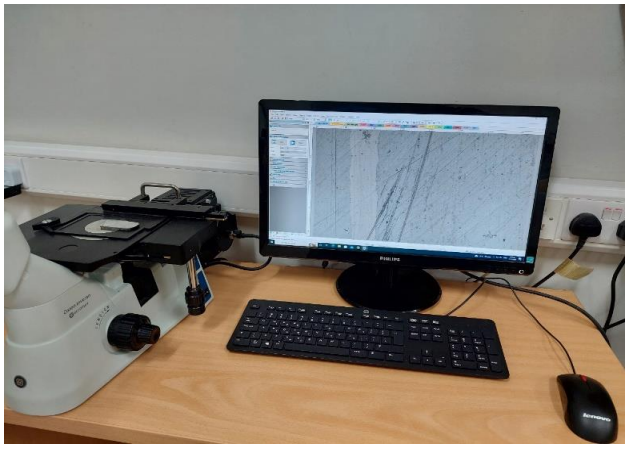

Figure 64: High resolution images of the interfaces could be obtained from the computer connected to the microscope

Figure 65: Sample placed on the microscope with the polished side facing down

From the images obtained from the microscope, the gap between the outer steel layer and the inner aluminium core of gear 2 is even more pronounced (*Figure 66*), while oxide residues can also be detected, as noted in *Figure 67*. The gap may be a result of oxides formed during heating, thermal expansion due to temperature differences between the two materials and even caused by the ejection forces that were applied during the manual ejection of the forged part. The materials of gear 8 seem close together, however the boundaries between the different materials are very clear, as seen in *Figure 68* and *Figure 69*. That means that the forging conditions of the experiments did not promote diffusion.

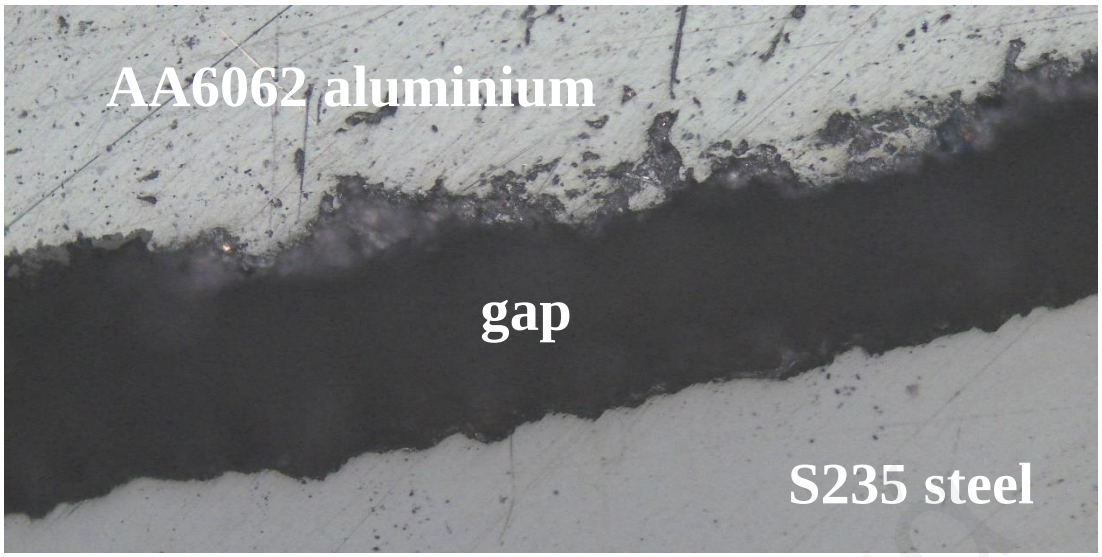

Figure 66: Gap in gear 2 interface

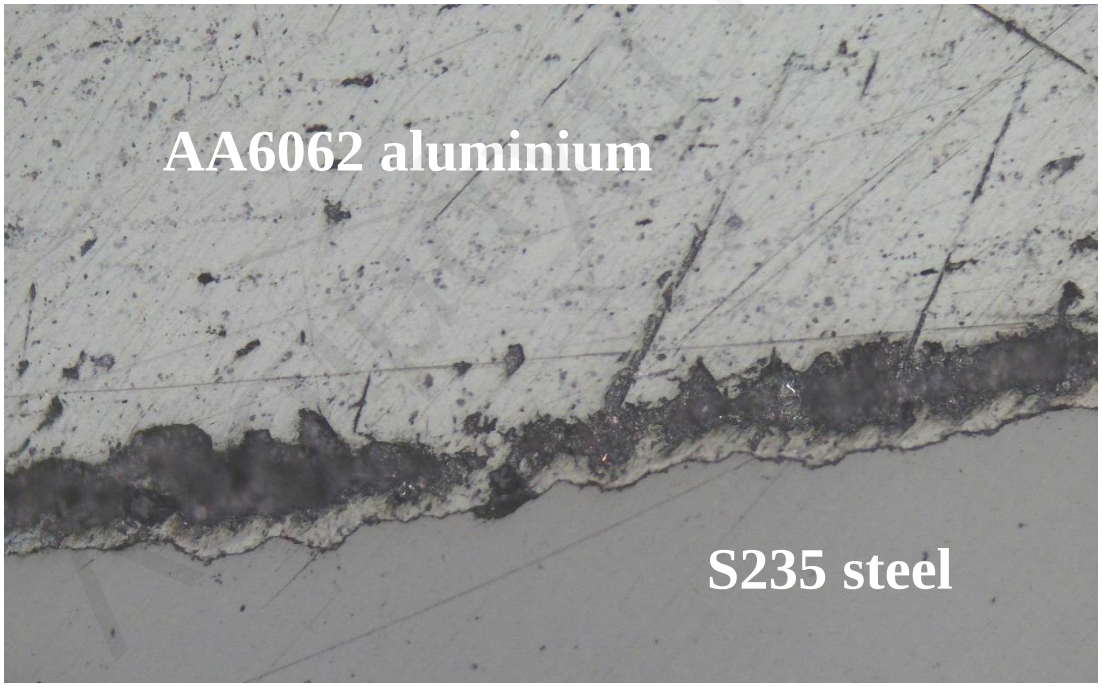

Figure 67: Oxide residues on the interface of gear 2

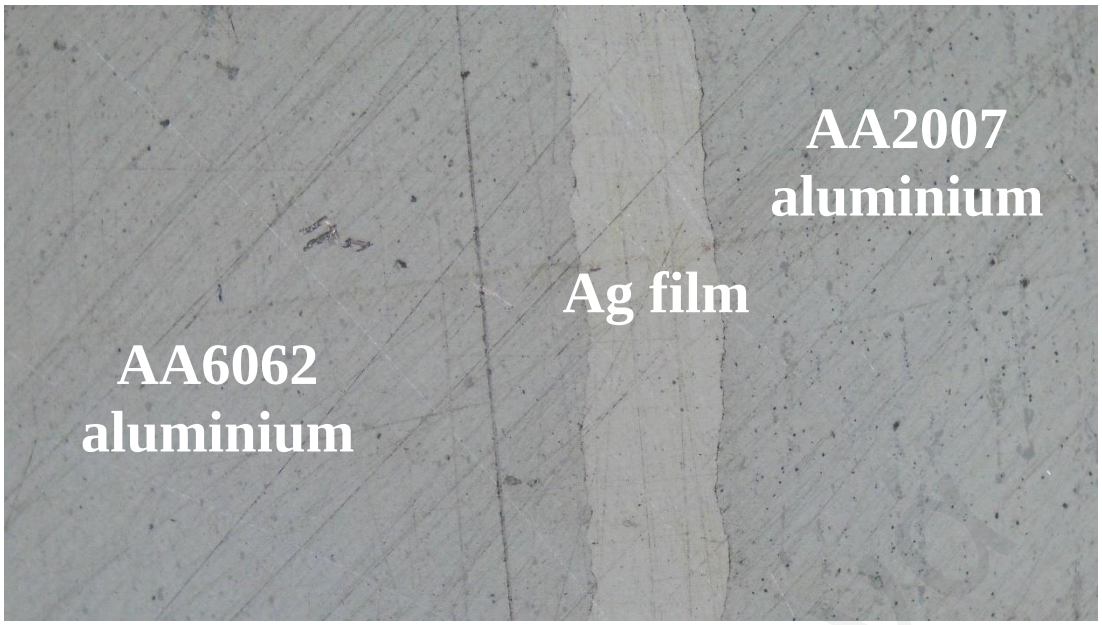

Figure 68: Silver film between AA6062 and AA2007

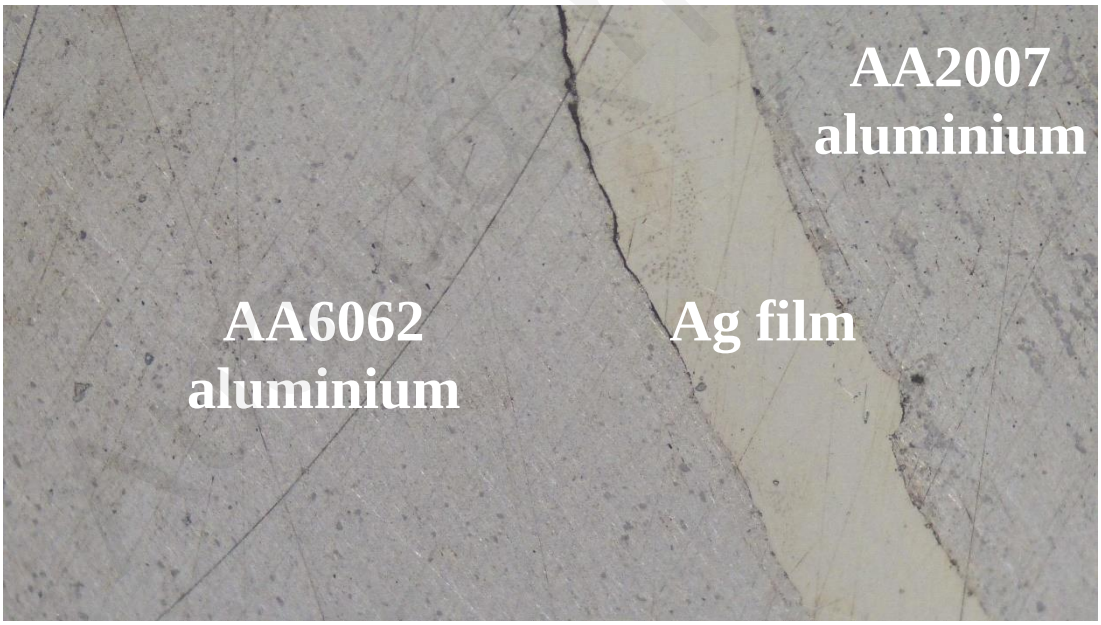

Figure 69: Small gaps detected in gear's 8 interface

2.4 Micro-hardness Testing

The sections from gear 2 and gear 8, after being observed under the optical microscope, were then placed on the CM-700 AT Clark Digital Micro-Hardness Tester. A Vickers indenter forms a square indent on the samples' surface, and the diagonals of the square indentation are measured with the micro-hardness tester, which then shows the Vickers hardness value on its digital screen. The Vickers hardness value was measured on specific areas and in particular on the AA6082-silver interface, AA2007-silver interface (*Figure 70*) and on the silver film, AA6082 and AA2007 parts of the sample of gear 8. For the sample of gear 2 (*Figure 72*), hardness values were only taken on the S235 (*Figure 71*) and AA6082 areas, since the gap between the materials did not make possible the indentation on their interface. The dwell time for all measurements was set to 15 seconds, while the load applied was set to be 100 g (0.9807 N) for all samples, except the steel part of the gear 2 section which was set to 10 g (0.09807 N), due to the sample tilting and causing a deformed indentation. Hardness testing with 100 g load was also carried out on the counterpunch, as seen in *Figure 73*, in order to study also the hardness of the forging toolset.

The average Vickers hardness value measured on the different areas is presented in the following *Table 13*. All the measurements taken can be found in *Appendix F*.

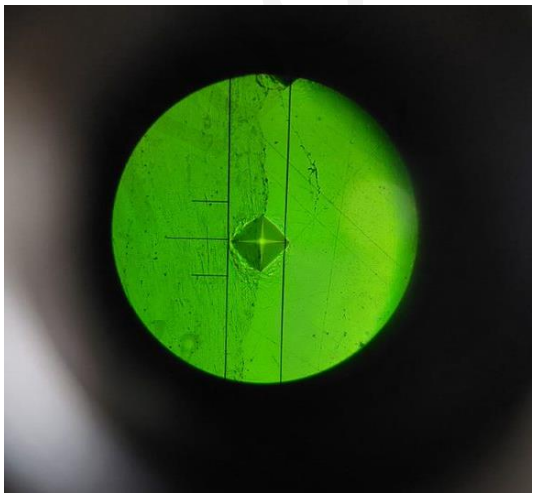

Figure 70: Vickers indentation on AA2007-Ag interface

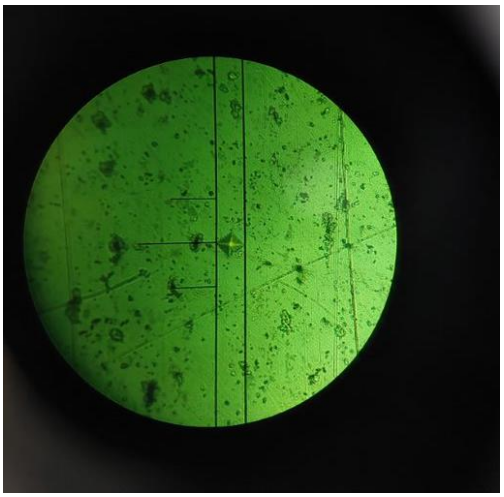

Figure 71: Vickers indentation on steel

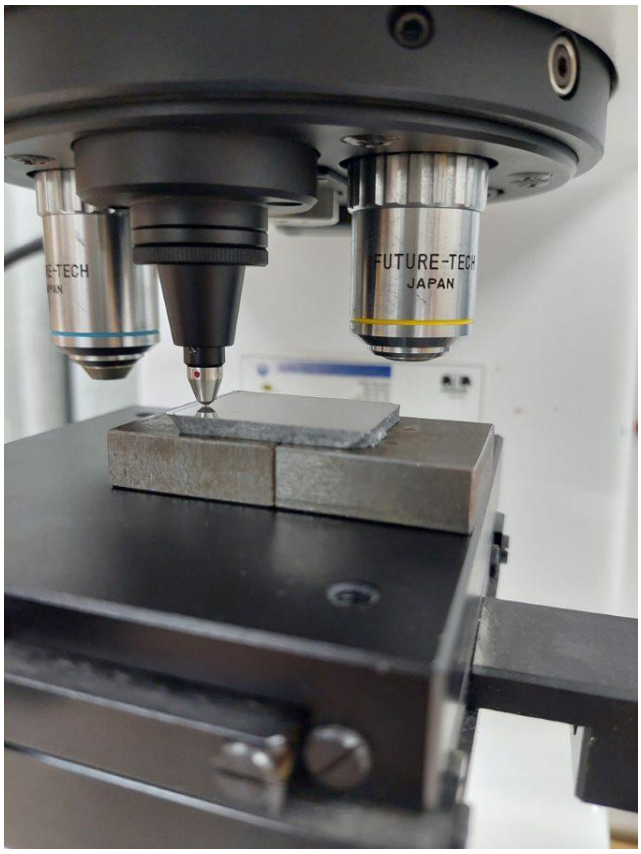

Figure 72: Vickers indenter on the section of gear 2

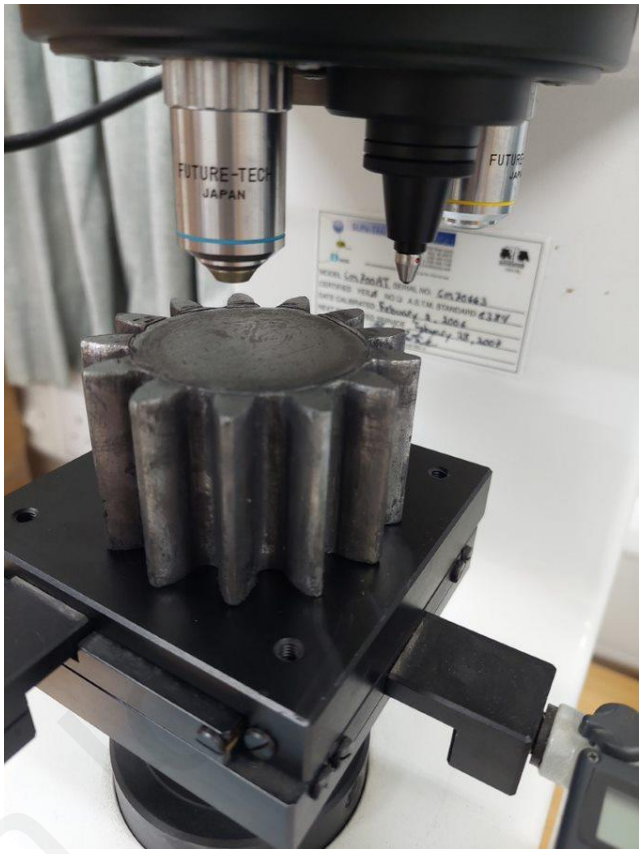

Figure 73: Micro-hardness testing on the counterpunch surface

Table 13: Average Vickers hardness value

	Average Vickers hardness (HV)
Gear 2: 1 mm S235 ring - Ø46 mm AA6082 core	
S235	178.1
AA6082	89.4
Gear 8:3 mm AA6082 ring - Ø42 mm AA2007 core – Ag film	
AA6082-Ag interface	78.1
AA2007-Ag interface	64.5
Ag	72.7
AA6082	105.6
AA2007	86.4
Counterpunch	
Mild steel	185.5

2.5 Challenges and Corrective Actions

During the experimental phase, a lot of unexpected challenges appeared. For some it was possible to make changes and take corrective actions to keep the experiments running smoothly, while for others, the needed improvements require different equipment or time-consuming processes, so they are intended for the future. The challenges and the corrective actions taken, wherever applicable, are listed below:

- The flash formation was expected to occur, therefore, to avoid the joining of the toolset parts, the punch was re-made with a smaller diameter, from $\emptyset 70\ mm$ to $\emptyset 50\ mm$, meaning that it no longer covered the die's teeth gaps. That was considered to allow flash to escape from the die's teeth gaps.

- The transportation of the samples from the SNOL furnaces to the die, causes the parts to cool. A simple solution was to raise the heating temperature of the samples from 900 °C and 500 °C, for steel and aluminium respectively, to 950 °C and 550 °C, to compensate for the heat loss during the conveyance.

- Prior to the actual experiments, a forging test was conducted with an aluminium cylinder of $\emptyset 50\ mm$ and $50\ mm$ height, which was firstly heated in a furnace and then placed inside the die to be forged. When pressing the part with the hydraulic press, it was noticed that the press reached a high force application very quickly, without the cylinder to be noticeably deformed. Then, it was observed that material was flowing over the die *(Figure 74)*, thus all samples had to be machined in order to reduce their height. The inner cores were machined to $40\ mm$ height from $50\ mm$, while the outer rings were machined to $37\ mm$ height from $45\ mm$.

- Initially the rings were machined to be of thickness of either 3 mm or 6 mm, but after the first experiment, the 3 mm S235 ring - Ø42 mm AA6082 core, was carried out and it was noted that the formed part was not sufficiently deformed, all the 6 mm rings were machined to be of 1 mm thickness. Their outer diameter remained the same, meaning that new aluminium cores had to be machined to Ø46 mm, in order to have the 1 mm clearance between the outer ring and the inner core.

Figure 74: Gear teeth could not be formed due to material flowing over the die

- When forging steel rings, it was noticed that during the re-assembly of the toolset, after the manual ejection of the forged part, the counterpunch did no longer fit inside the die. The deformed parts were machined whenever it was required, in order to be able to be used again for the following experiments. Damage caused by the forging of the metal samples can be detected on the upper surface of the counterpunch, as seen in *Figure 75*.

Figure 75: Damage on counterpunch

Figure 76: Deformation of pillar

- Initially the rings were machined to be of thickness of either 3 mm or 6 mm, but after the first experiment, the 3 mm S235 ring - Ø42 mm AA6082 core, was carried out and it was noted that the formed part was not sufficiently deformed, all the 6 mm rings were machined to be of 1 mm thickness. Their outer diameter remained the same, meaning that new aluminium cores had to be machined to Ø46 mm, in order to have the 1 mm clearance between the outer ring and the inner core.

- The alignment tool was also machined after a few experiments, with its top part, responsible for the alignment, being completely removed because it could not fit together with the counterpunch. The continuous temperature changes, might have caused the thermal expansion of the part, making it unable to fit with the counterpunch.

- It was noticed that the toolset was gradually bending during forging and resulting in the deformation of the back smaller pillar. It was observed that the thread on its top was deformed to the point that the nut placed to secure the ring could not fit anymore, as seen in *Figure 76*. No corrective actions were taken, but a better design for the die on springs is suggested for future improvements.

- The application of the films on the outer rings was challenging for the assembly of the outer ring and the inner core when they were placed inside the die. The solid interlayer could not fit perfectly around the inner surface of the outer ring, reducing the 1 mm clearance between the two, and allowing air to be present between the film and the ring. Alternatively, CVD or PVD coats can be applied instead of solid interlayers.

Chapter 3

3 CONCLUSIONS

3.1 Conclusions

Through analysis and interpretation of the results coming from the forging experiments, the microhardness tests and the images obtained from the optical microscope, several key findings have emerged, highlighting the importance of the forging conditions and the appropriate equipment. These conclusions not only contribute to our understanding of the production of lightweight multi-metal gears with forging, but also have significant implications for the better bonding of the dissimilar metals.

The conclusions are outlined in the following points:

- The capacity of the hydraulic press did not allow the filling of the sharp gear teeth geometry of the die. For the same hydraulic press, it is advised to use a gear shape of smaller module.

- To achieve greater deformation, it was necessary to anneal all the aluminium samples that were used during the experiments.

- For experiments with the same material combination, it was noticed that the initial experiments required additional force compared to the latter ones, however the deformation and the final sample dimensions that were noted were very similar. The extra amount of force that was applied during the initial experiments was probably responsible for the bending and deformation of the toolset.

- The application of the copper and silver films was challenging due to their thickness, which made it difficult for them to bend and fit on the curved surface of the outer ring. The air gaps that were formed between the film and the outer ring made the material bonding more difficult. However, as seen from the

experimental results, the solid interlayer worked better for similar metals (AA6082 – AA2007 combination).

- The detachment of the outer layer of the gears when they were cut in the Bemato Sawing machine, may be a result of the ejection forces that were applied during the ejection of the forged part in the manual press and the friction that was caused due to the contact of the outer layer to the die. Additionally, the formed oxides prevented the metal-to-metal contact, leading to a weak intermetallic bond.

- The temperature difference and the heat cycles that the toolset was submitted to caused thermal expansion to the toolset and then machining of the toolset parts was required. A different toolset material, that is less prone to thermal expansion from temperature difference, may be a better solution for these experiments.

- The clear material boundaries on the interface of gear 8, that were observed with the optical microscope, indicate that the experimental conditions were not favorable for diffusion bonding.

- The hardness of the toolset was found to be similar to the hardness of the S235 sample. This finding justifies the damage that was caused on the toolset, and especially on the upper surface of the counterpunch. Since the forging toolset was made from mild steel, a higher strength steel might be a better solution when forging S235 steel samples.

- Compared to the manufacturing of a gear made solely from a S235 cylinder, a 46.61% weight reduction could be achieved when manufacturing a gear with aluminium core and a 3mm outer steel ring and a 61.05% weight reduction could be achieved when manufacturing a gear with aluminium core and a 1mm outer steel ring. Thus, the production of multi-metal gears leads to significant weight reduction.

Chapter 4

4 FUTURE WORK

4.1 Future Work

While this study has significantly improved our understanding of the manufacturing of lightweight multi-metal gears, further investigation and improvements are required to address the achievement of a strong intermetallic bond between the different materials and the production of a functional multi-metal gear. The following section outlines potential directions for future work, aiming to expand upon the finding of this study.

Future work suggestions are presented in the points below:

- Re-making of the punch, die and counterpunch from a high strength steel is important in order to withstand the deformation caused by the metal samples.
- A different gear geometry is suggested for the manufacturing of the gears using the particular hydraulic press, to achieve the desired deformation.
- Re-designing of the die on springs mechanism using a uniform structure instead of pillars, to avoid the deformation and bending of the toolset.
- Installation of an ejection system on the hydraulic press to avoid the disassembly of the toolset to remove the joined parts and the manual ejection of the forged part and the uncontrolled ejections forces that are applied.
- Use an inert gas atmosphere inside the furnaces to avoid the formation of oxides during the heating of the samples.
- Changing the film application method to a PVD or CVD coating on the metal samples, to prevent the air gaps and poor fitting of the solid interlayers.
- Automation of the forging process in order to have a constant force application for all the experiments.

References

[1] Oda S, Mlyachika K, Sayama T (1986) Effects of rim and web thicknesses on bending fatigue strength of internal gear. Bull JSME 29(248):586–592D.R. Fulkerson and O.A. Gross, "Incidence matrices and interval graphs", *Pacific J. Math*, vol. 15, pp. 835-855, 1965

[2] Sayama T, Oda S, Umezawa K (1986) Study on welded structure gears: 11th report, optimum structure for thin-rimmed spur gear. Bull JSME 29(256):3582–3586

[3] Opalić, M., Vučković, K. and Kljajin, M. (2011) January. Effect of Web Arrangement on Thin-Rim Gear Tooth Contact Stress. In 15th International Research/Expert Conference-Trends in the Development of Machinery and Associated Technology, Prague, Czech Republic, 545–548.

[4] Abdel-Rahman ARO, Dean TA (1981) The quality of hot forged spur gear forms. Part I: Mechanical and metallurgical properties. Int J Mach Tool Design Res 21(2):109–127

[5] Chavdar B, Goldstein R, Yang X, Butkovich J, Ferguson L (2015) Hot Hydroforging for Lightweighting. 5th International Conference on Distortion Engineering, 23–25 September, Bremen, Germany.

[6] Meißner R, Liewald M, Benkert T, Volk W (2017) Lightweight gearwheel design using separate gear ring and wheel body Part II: Different manufacturing concepts for replacing a full body gearwheel. 5th International Conference on Steels in Cars and Trucks. 18–22 June, Amsterdam, The Netherlands.

[7] Hirschvogel Automotive Group (2020) Gear Lightweighting Idea. Available online at: https://www.hirschvogel.com/en/products/transmission/gear-lightweighting-idea

[8] MTI Inc. (2020) Two pre-finished transmission gears welded using precision piloted tool. Available online at: https://www.mtiwelding.com/parts/?materials=steel-low-carbon-alloy-gearsteel

[9] Miller WH (1974) Gear Blanks, Patent No. U.S. 3,847,557, November 12.

[10] Tekkaya AE (2012) Recent developments in bulk metal forming. In: Ishikawa T, Yoshida Y, Hayakawa K, Wang Z (Eds.), Proceedings of the 45th ICFG Plenary Meeting (ICFG2012), 57–77.

[11] Groche P, Wohletz S, Brenneis M, Pabst C, Resch F (2014) Joining by forming—a review on joint mechanisms, applications and future trends. J Mater Process Technol 214(10):1972–1994

[12] Ossenkemper S, Dahnke C, Tekkaya AE (2019) Analytical and experimental bond strength investigation of cold forged composite shafts. J Mater Process Technol 264:190–199

[13] Lätzer M, Kleditzsch S, Leidich E, Awiszus B (2012) Analytical and numerical computation of knurled interference fits in comparison with experimental studies. IMEKO TC15 – Experimental Mechanics – Proceedings of the 11th Youth Symposium on Experimental Solid Mechanics, 112–117.

[14] Qiao J, Kou SQ, He DY, Yang SH (2008) Torque strength and influencing factors analysis for assembled camshaft by knurling joining. MSF 575:216–221

[15] Chugreeva A, Mildebrath M, Diefenback J, Barroi A, Lammers M, Hermsdorf J, Hassel T, Overmeyer L, Behrens BA (2018) Manufacturing of high-performance bi-metal bevel gears by combined deposition welding and forging. Metals 8:898

[16] Behrens BA, Diefenbach J, Chugreeva A, Kahra C, Herbst S, Nurnberger F (2020) Tailored forming of hybrid bevel gears with integrated heat treatment. Procedia Manuf 47:301–308

[17] Ding Y, You G, Wen H, Li P, Tong X, Zhou Y (2019) Microstructure and mechanical properties of inertia friction welded joints between alloy steel 42CrMo and cast Ni-based superalloy K418. J Alloy Compd 803:176–184

[18] Wu P, Wang B, Lin J, Zuo B, Li Z, Zhou J (2017) Investigation on metal flow and forming load of bi-metal gear hot forging process. Int J Adv Manuf Technol 88:2835–2847

[19] Politis DJ, Lin J, Dean TA (2012) Investigation of Material Flow in Forging Bi-metal Components. Steel Research International. Proceedings of the 14th international Conference on Metal Forming. 231, 234.

[20] Politis DJ, Lin J, Dean TA, Balint DS (2014) An investigation into the forging of Bi-metal gears. J Mater Process Technol214(11):2248–2260

[21] Bhushan B (2003) Adhesion and stiction: mechanisms, measurement techniques, and methods for reduction. J Vac Sci Technol B 21(6):2262–2296

[22] Bhushan B (2003) Adhesion and stiction: mechanisms, measurement techniques, and methods for reduction. J Vac Sci Technol B 21(6):2262–2296

[23] Rabinowicz E (1995) Adhesive wear. Friction and Wear of Materials, 2nd edn. Wiley, New York

[24] Kalpakjian S, Schmid SR (2006) Manufacturing, engineering and technology, 5th edn. Pearson Education Inc., New Jersey

[25] Chen RY, Yuen WYD (2000) A study of the scale structure of hot-rolled steel strip by simulated coiling and cooling. Oxid Met 53(5):539–560

[26] Crane CH, Lovell DT, Baginski WA, Olsen MG (1967) Diffusion welding of dissimilar metals. Weld J 46(1):S23

[27] Dybkov VI (1990) Interaction of 18Cr-10Ni stainless steel with liquid aluminium. J Mater Sci 25(8):3615–3633

[28] Ghosh M, Bhanumurthy K, Kale GB, Krishnan J, Chatterjee S (2003) Diffusion bonding of titanium to 304 stainless steel. J Nucl Mater 322(2):235–241

[29] Owczarski W (1981) Application of diffusion welding. US Weld J 60(2):22–33

[30] Awiszus B, Neugebauer R, Kittner K, Popp M (2009) Analyse des Quer-fließpressens als Analogieversuch zum Strangpressen unter besondererBerücksichtigung der Verbundbildung zwischen Aluminium und Magnesium. UTF Sci Online J 4:1–18

[31] Hack HP (2016) Module in materials science and materials engineering. Elsevier, Amsterdam

[32] Gottstein G (2004) Physical foundations of materials science. Springer, Berlin

[33] Zhang W, Bay N (1997) Cold welding-theoretical modeling of the weld formation. Weld J Includ Weld Res Suppl 76(10):477s

[34] Tan YH, Lee SL, Wu HY (1996) Effects of beryllium on fatigue crack propagation of A357 alloys containing iron. Int J Fatigue 18(2):137–147

[35] Assadi H, Shirzadi AA, Wallach ER (2001) Transient liquid phase diffusion bonding under a temperature gradient: modelling of the interface morphology. Acta Mater 49(1):31–39

[36] Dray AE (1985) Diffusion bonding of aluminium. Doctoral dissertation, University of Cambridge

[37] Bay N (1983) Mechanisms producing metallic bonds in cold welding. Weld J 62:137–142

[38] Kazakov NF (1985) Diffusion bonding of Materials. Pergamon Press, Oxford (ISBN: 978-0-08-032550-7)

[39] Nicholas MG, Crispin RM (1982) Diffusion bonding stainless steel to alumina using aluminium interlayers. J Mater Sci 17(11):3347–3360

[40] Muktepavela F, Maniks J (2003) Mechanical properties of deformed interfaces in bimetallic joints. Solid State Phenom Trans Tech Publ 94:79–84

[41] Politis NJ (2017) Forging Lightweight Bimetal Gears. Doctoral Dissertation. Imperial College London, UK

[42] Behrens BA, Kosch KG, Frischkorn C, Vahed N, Huskic A (2012) Compound forging of hybrid powder-solid-parts made of steel and aluminum. KEM 504–506:175–180

[43] Szczepanik S, Nikiel P (2012) Some aspects of extrusion of two-layers PM materials. In: Kusiak, J. (Ed.), Metal Forming 2012, Proceedings of the 14th International Conference on Metal Forming. September 16–19, 2012. AGH Univ. of Science and Technology, Krakow, Poland, 475–478.

Appendices

Appendix A - YQ41-100 Hydraulic Press Characteristics

The YQ41-100 press (Machine number 210110 and Ex. Factory Date 09.2021) is an all-steel welded structure. The hydraulic control is achieved by using a two-way cartridge valve integrated system. Its performance characteristics can be found in the following table:

Table VI: YQ41-100 Hydraulic Press characteristics

Parameters	
Nominal Force	$1000\ kN$
Working pressure	$19\ MPa$
Ram stroke	$320\ mm$
Opening height	$700\ mm$
Throat depth	$280\ mm$
Approaching speed	$50\ mm/s$
Pressing speed	$8\ mm/s$
Return speed	$13\ mm/s$
Working table size (L-R)	$700\ mm$
Working table size (F-B)	$500\ mm$
Blacking hole diameter	$200\ mm$
Weight	$3500\ kg$
Overall size (L×W×H)	$1380 \times 800 \times 2120\ mm$
Motor power	$5.5\ kW$

Appendix B – Model Names of Basic Toolset

The basic toolset is the ‘Eco-Line’ Steel Die Set without stripper from Fibro, and it consists of a top and bottom plate (mentioned together as die set), two press-fitted guide pillars with their respective high-performance compression springs and two guide bushes without stripper. Additionally, three Fibro high-performance compression springs are purchased for the three smaller guide pillars.

Table II: Model names of toolset parts

Part	Amount	Model number
Die set	1	2010.55.5031.1
Press-fitted guide pillar (taller)	2	202.29.030.400
High-performance compression spring (bigger)	2	241.14.63.305
Guide bushes without stripper	2	2081.94
High-performance compression spring (smaller)	3	241.14.40.152

Appendix C – Engineering Drawings of Basic and Forging Toolset

In this section, the engineering drawings of the punch, die, counterpunch and alignment tool are presented. The exploded view of the whole toolset assembly and the Bill of Materials are also presented in the following pages.

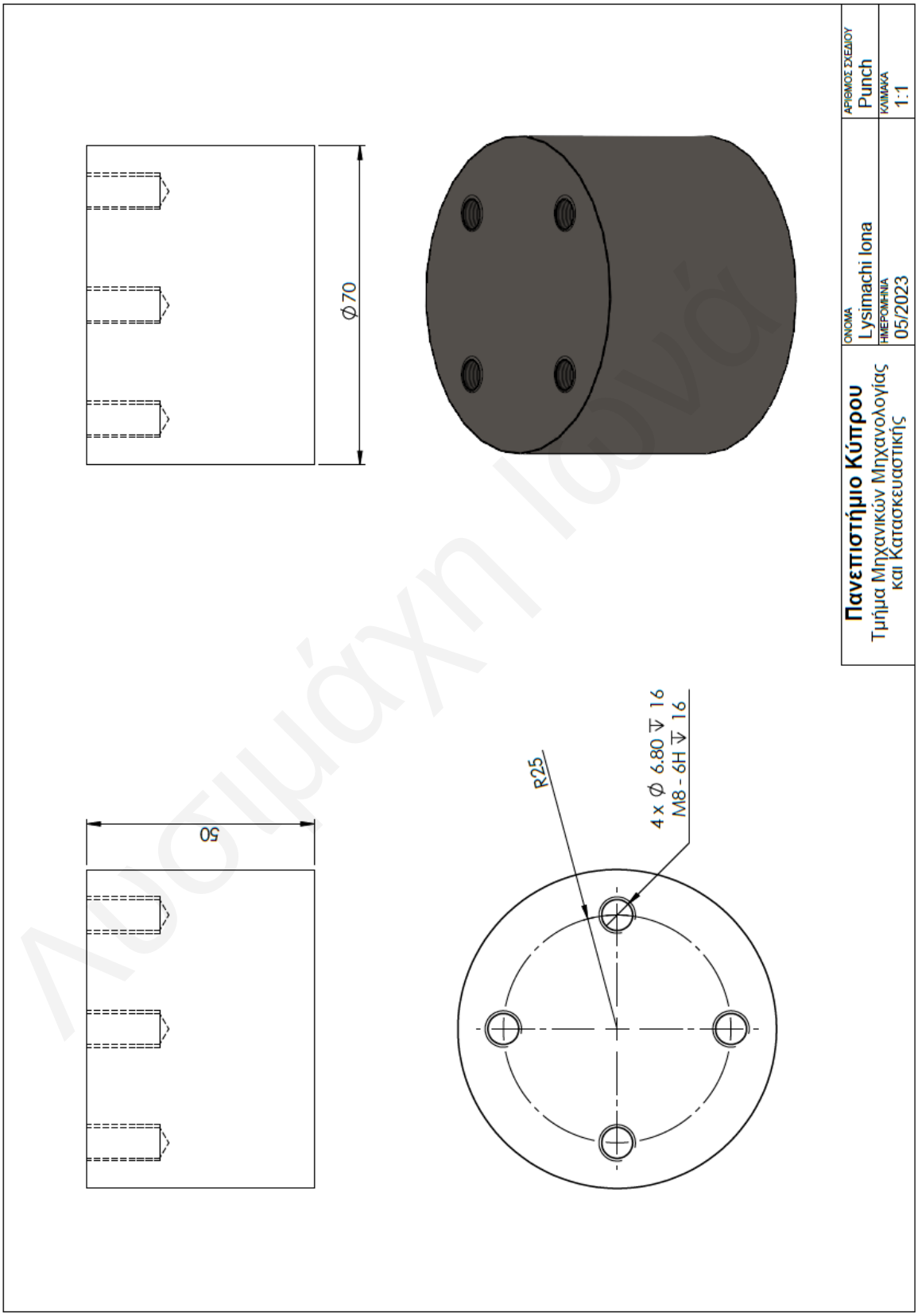
Ø70
50
R25
4 x Ø 6.80 ↧ 16
M8 - 6H ↧ 16
Πανεπιστήμιο Κύπρου
Τμήμα Μηχανικών Μηχανολογίας
και Κατασκευαστικής
ΟΝΟΜΑ
Lysimachi Iona
ΗΜΕΡΟΜΗΝΙΑ
05/2023
ΑΡΙΘΜΟΣ ΣΧΕΔΙΟΥ
Punch
ΚΛΙΜΑΚΑ
1:1

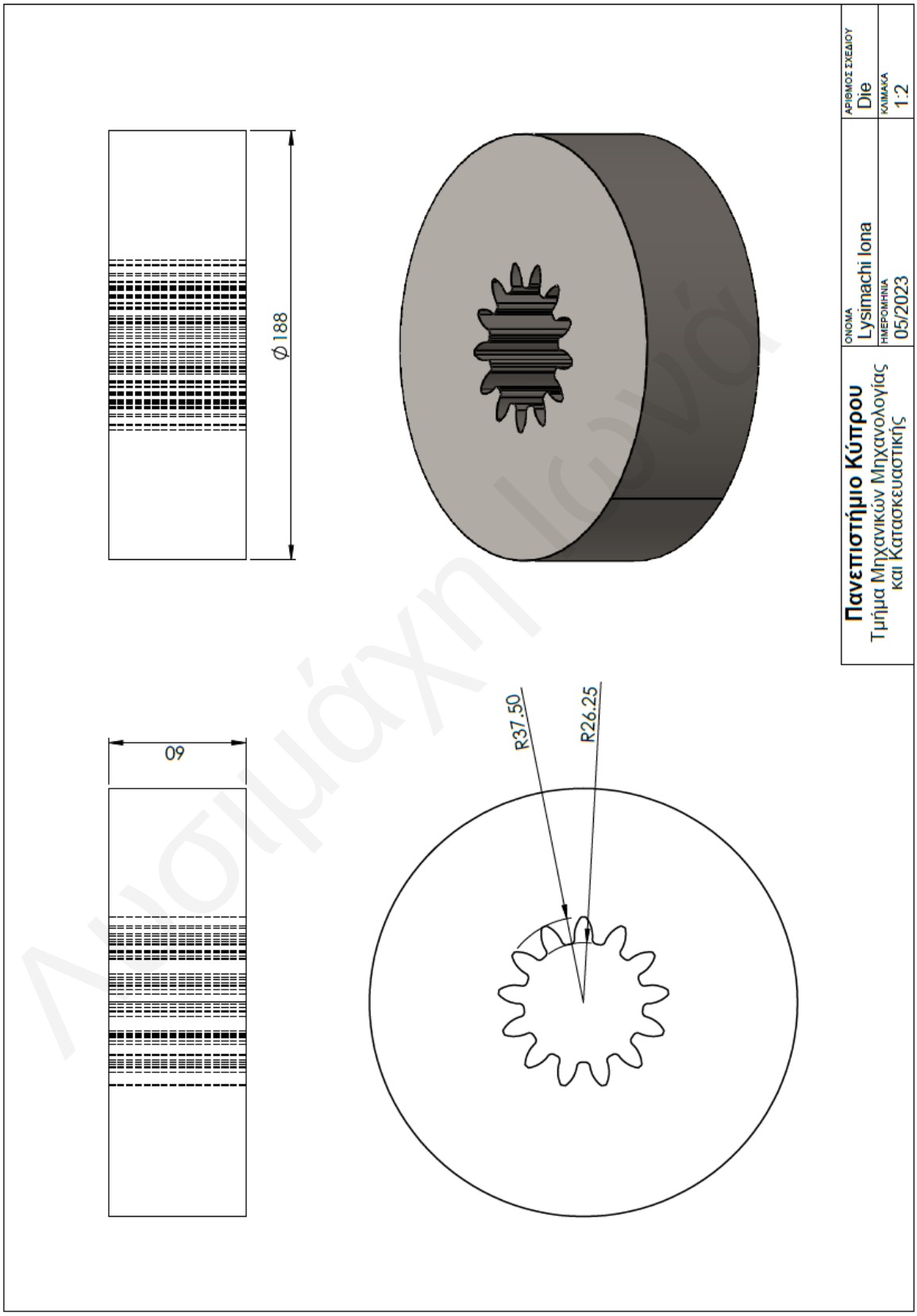
Ø188
60
R37.50
R26.25
Πανεπιστήμιο Κύπρου
Τμήμα Μηχανικών Μηχανολογίας
και Κατασκευαστικής
ΟΝΟΜΑ
Lysimachi Iona
ΗΜΕΡΟΜΗΝΙΑ
05/2023
ΑΡΙΘΜΟΣ ΣΧΕΔΙΟΥ
Die
ΚΛΙΜΑΚΑ
1:2

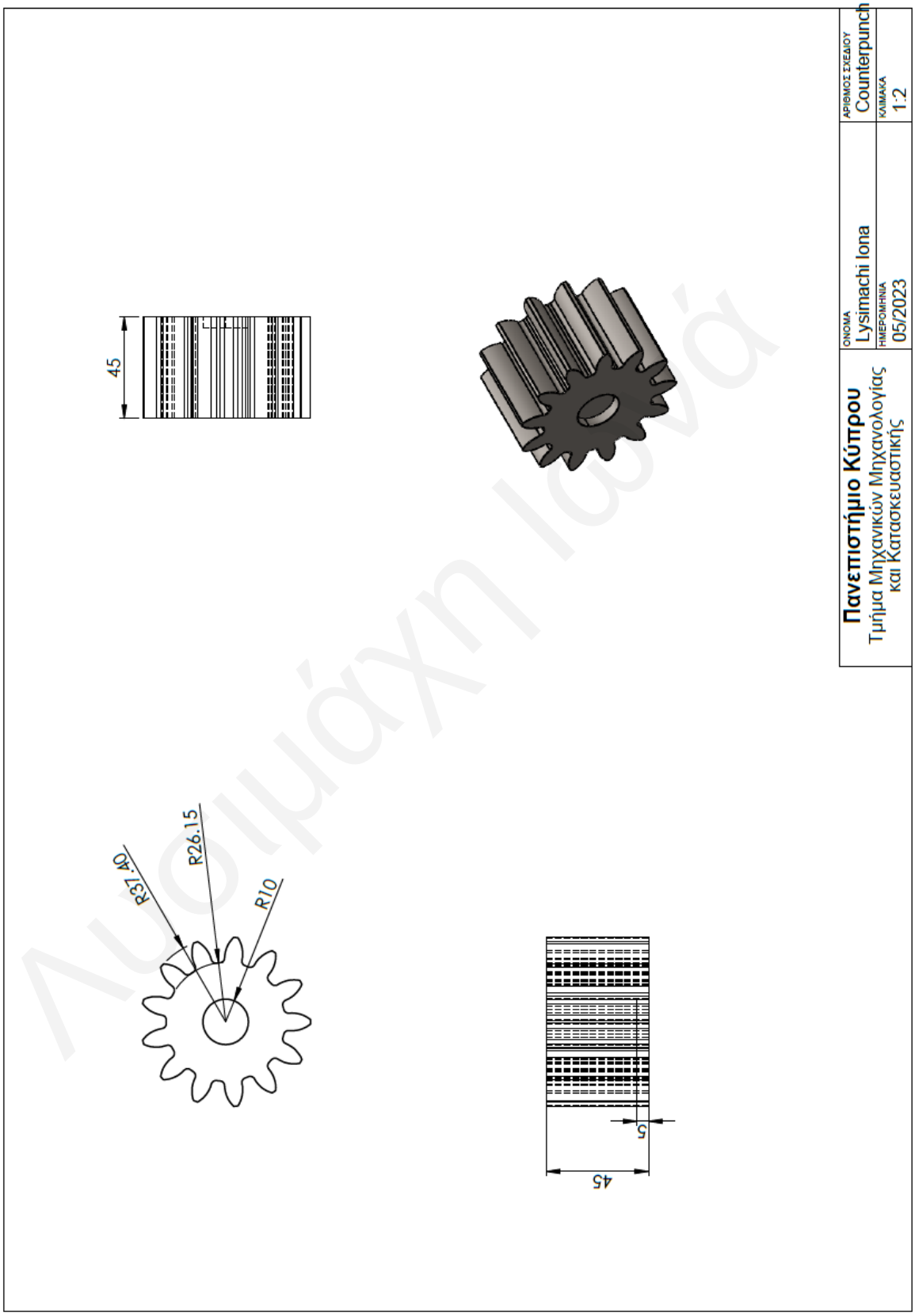
45
R31.40
R26.15
R10
5
45
Πανεπιστήμιο Κύπρου
Τμήμα Μηχανικών Μηχανολογίας και Κατασκευαστικής
ΟΝΟΜΑ
Lysimachi Iona
ΗΜΕΡΟΜΗΝΙΑ
05/2023
ΑΡΙΘΜΟΣ ΣΧΕΔΙΟΥ
Counterpunch
ΚΛΙΜΑΚΑ
1:2

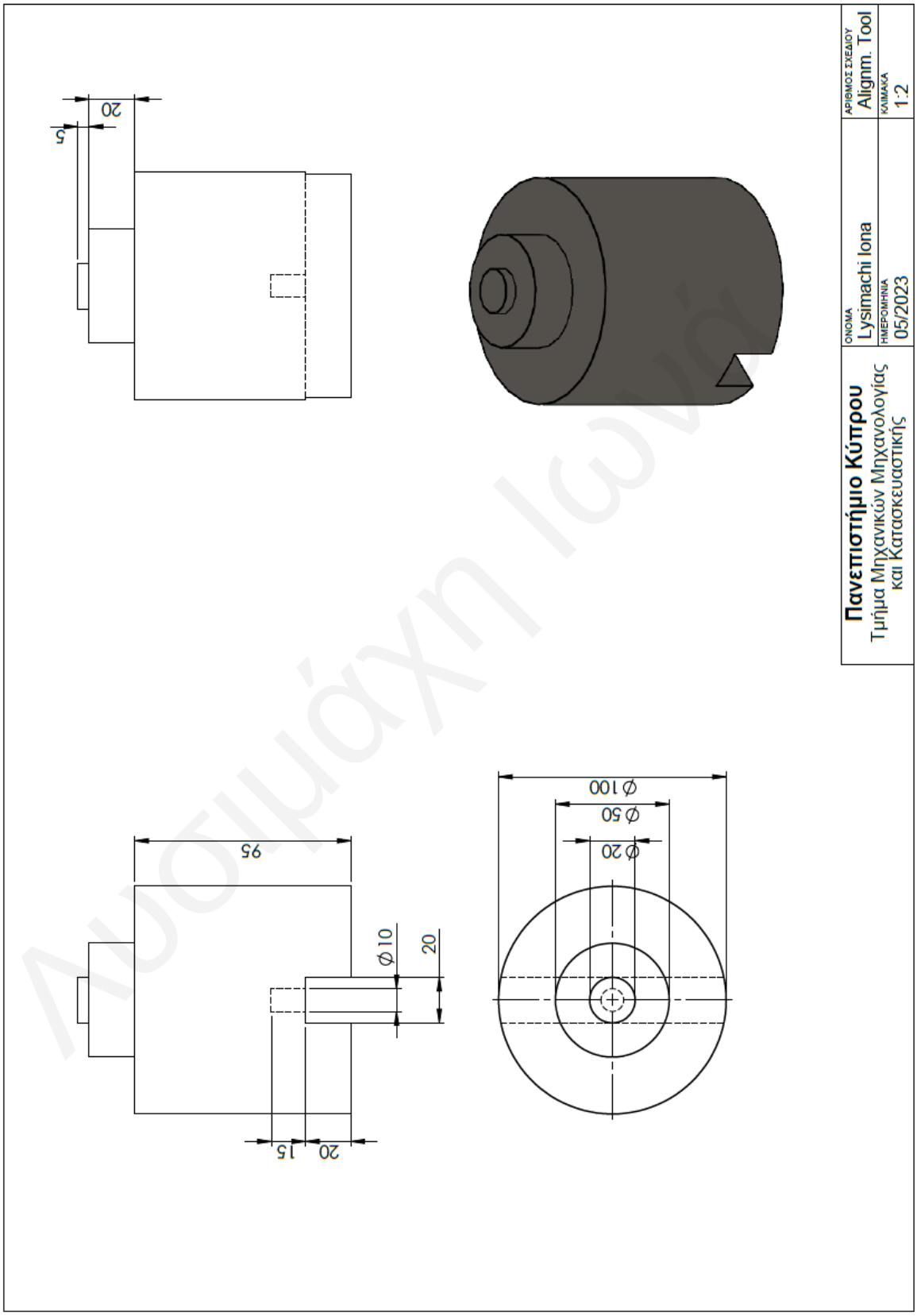
20
5
95
Ø10
20
15
20
Ø100
Ø50
Ø20
Πανεπιστήμιο Κύπρου
Τμήμα Μηχανικών Μηχανολογίας και Κατασκευαστικής
ΟΝΟΜΑ
Lysimachi Iona
ΗΜΕΡΟΜΗΝΙΑ
05/2023
ΑΡΙΘΜΟΣ ΣΧΕΔΙΟΥ
Alignm. Tool
ΚΛΙΜΑΚΑ
1:2

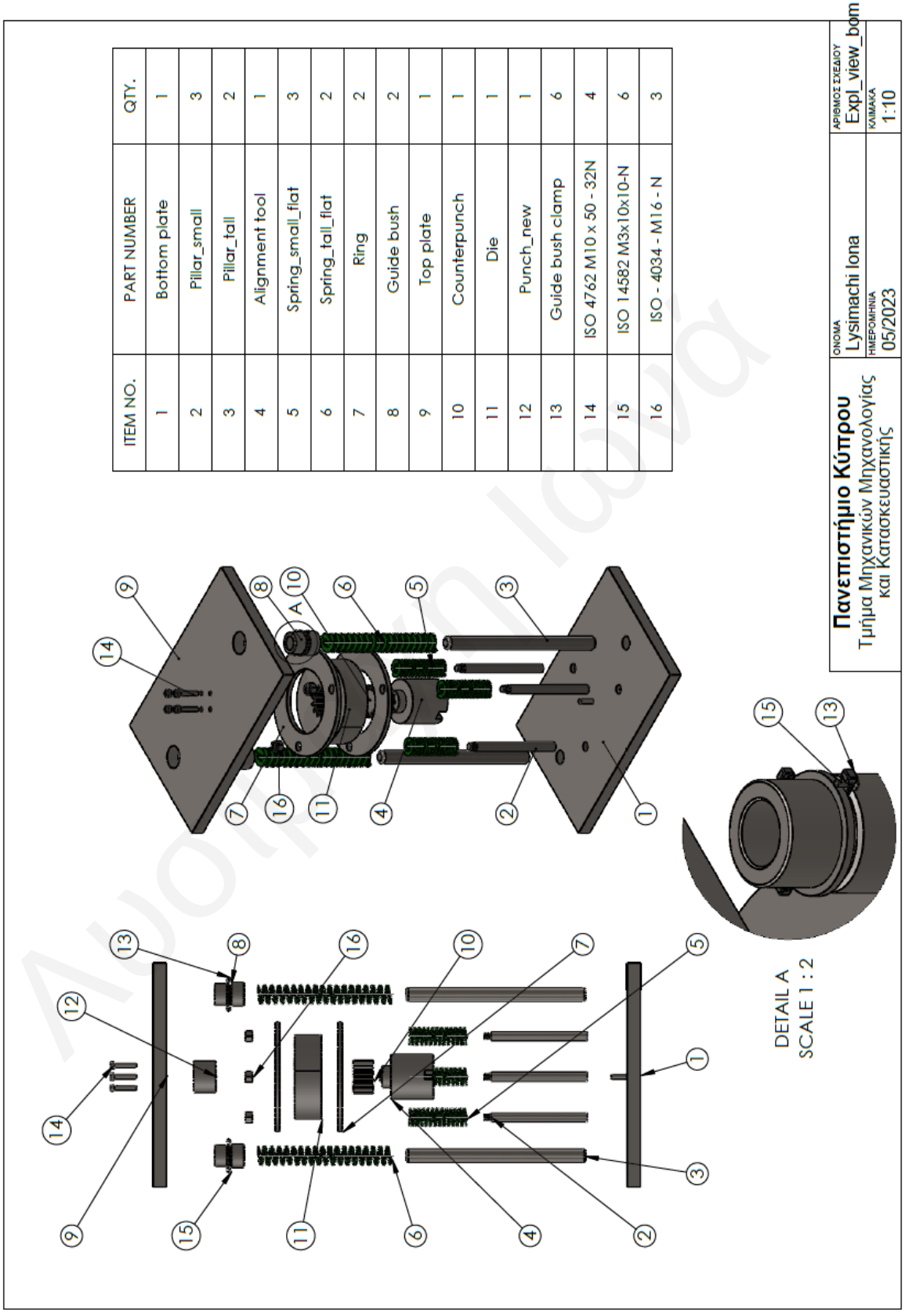
ITEM NO. | PART NUMBER | QTY.
1 | Bottom plate | 1
2 | Pillar_small | 3
3 | Pillar_tall | 2
4 | Alignment tool | 1
5 | Spring_small_flat | 3
6 | Spring_tall_flat | 2
7 | Ring | 2
8 | Guide bush | 2
9 | Top plate | 1
10 | Counterpunch | 1
11 | Die | 1
12 | Punch_new | 1
13 | Guide bush clamp | 6
14 | ISO 4762 M10 x 50 - 32N | 4
15 | ISO 14582 M3x10x10-N | 6
16 | ISO - 4034 - M16 - N | 3
Πανεπιστήμιο Κύπρου
Τμήμα Μηχανικών Μηχανολογίας και Κατασκευαστικής
ΟΝΟΜΑ Lysimachi Iona
ΗΜΕΡΟΜΗΝΙΑ 05/2023
ΑΡΙΘΜΟΣ ΣΧΕΔΙΟΥ Expl_view_bom
ΚΛΙΜΑΚΑ 1:10
DETAIL A
SCALE 1 : 2

Appendix D - Code and Explanation of Arduino Sketch

```
// Green cable connected to GND and brown to A0

const int analogInPin = A0;  // Analog input pin that the potentiometer is attached to

int sensorValue = 0;        // value read from the pot

void setup() {
  // initialize serial communications at 9600 bps:
  Serial.begin(9600);
}

void loop() {
  // read the analog in value:
  sensorValue = analogRead(analogInPin);

  sensorValue = map(sensorValue, 1023, 0, 200, 600);
  // print the results to the Serial Monitor:
 // Serial.print("sensor = ");
  Serial.println(sensorValue);

  delay(100);
}
```

Appendix E – Plots from Sensor Data

Experiment 1: 3 mm S235 ring - ∅42 mm AA6082 core

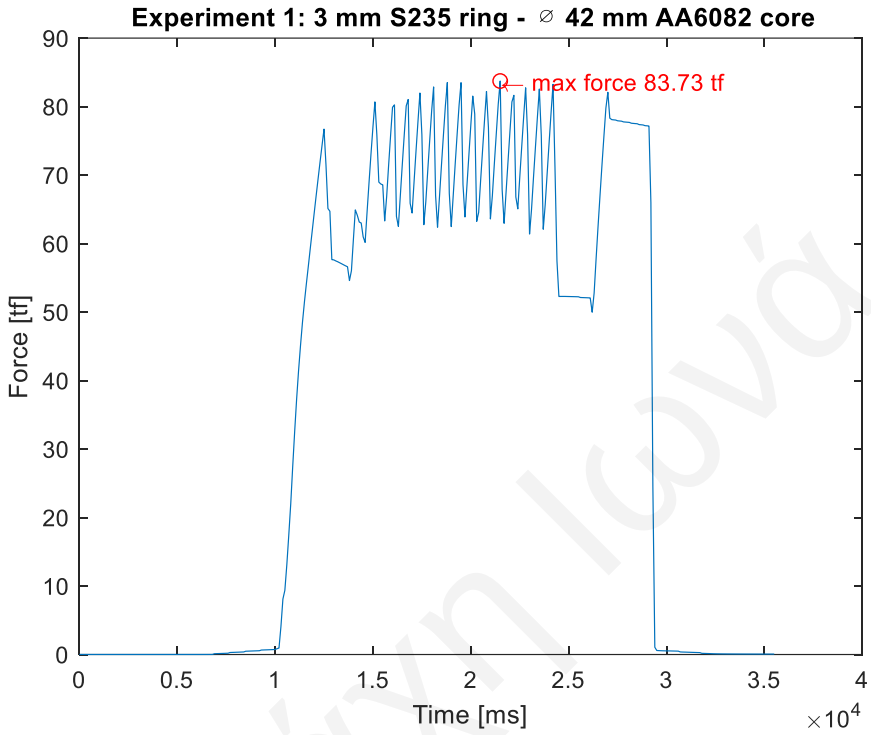

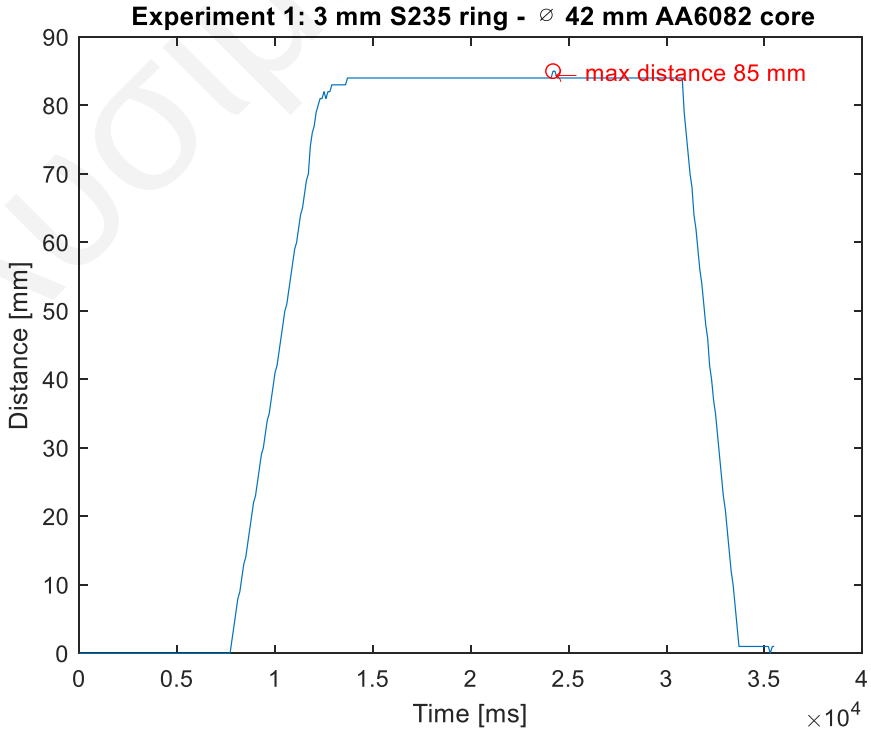

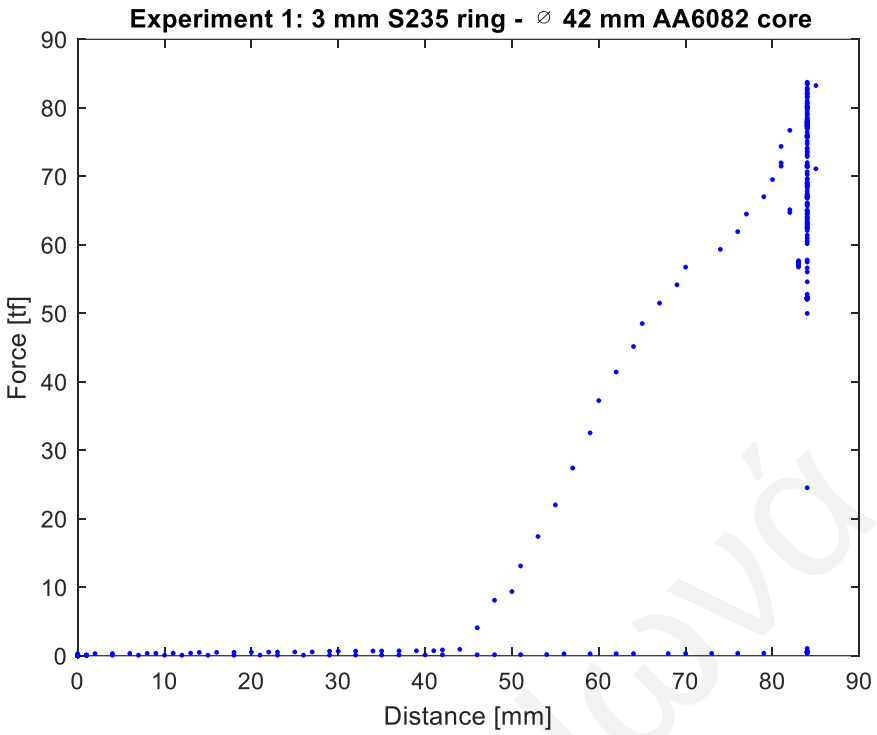

Experiment 2: 1 mm S235 ring - Ø46 mm AA6082 core

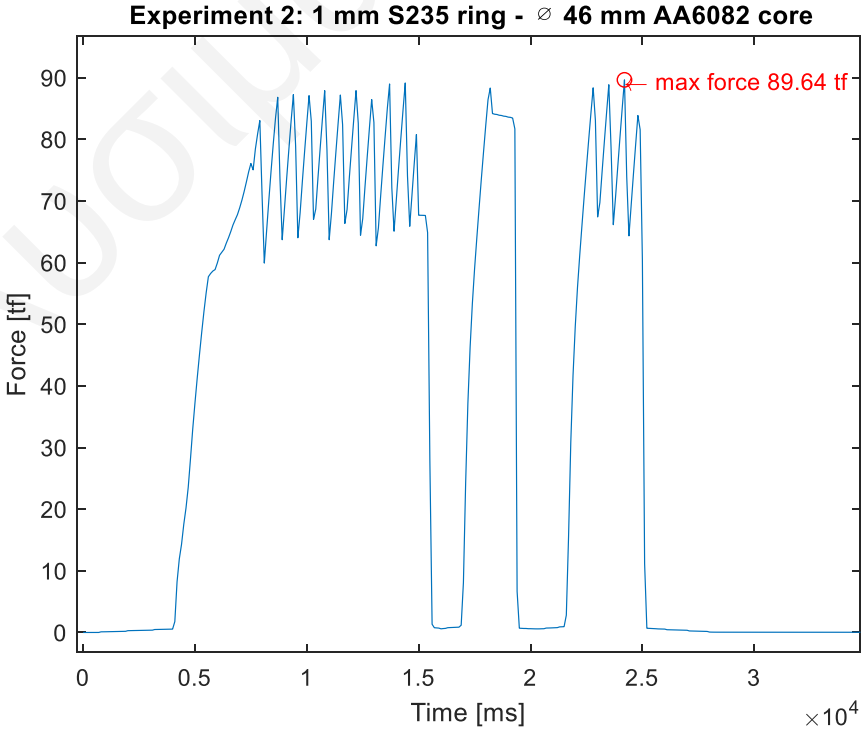

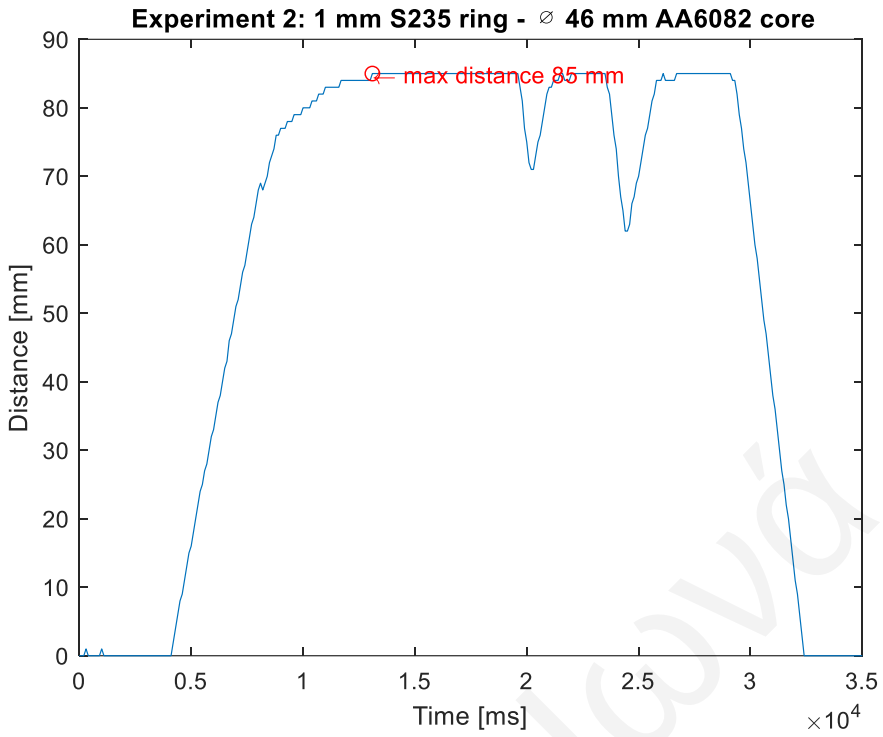

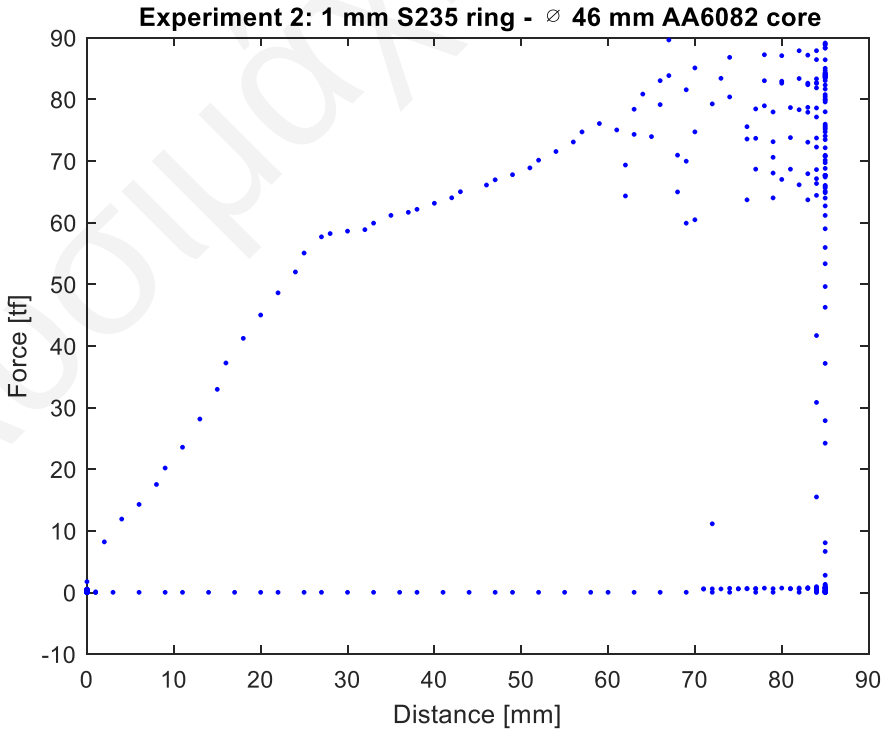

Experiment 3 and 6: 3 mm AA6082 ring - Ø42 mm AA2007 core

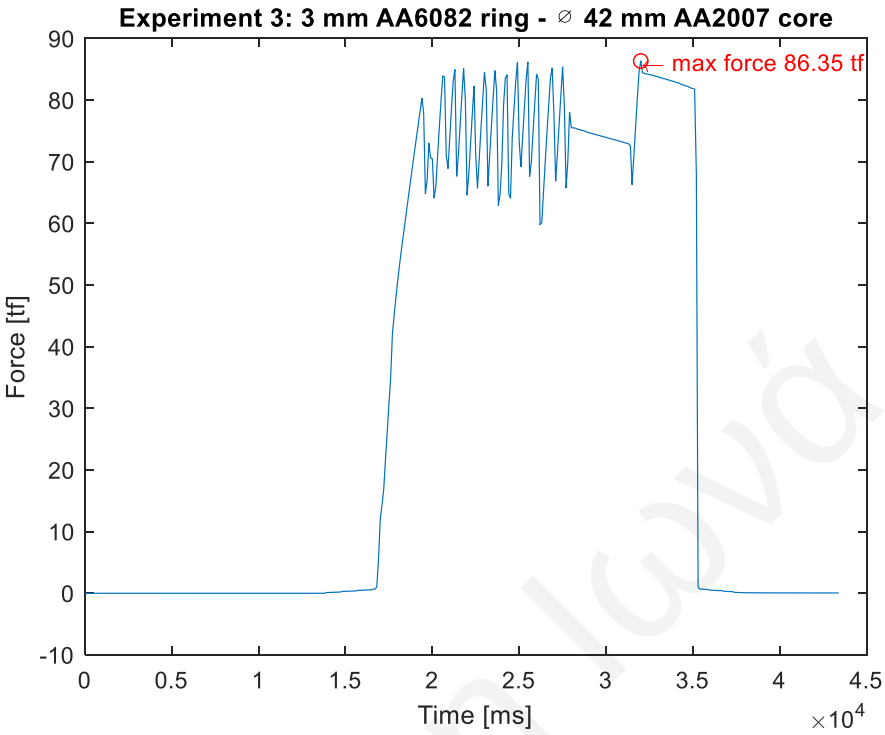

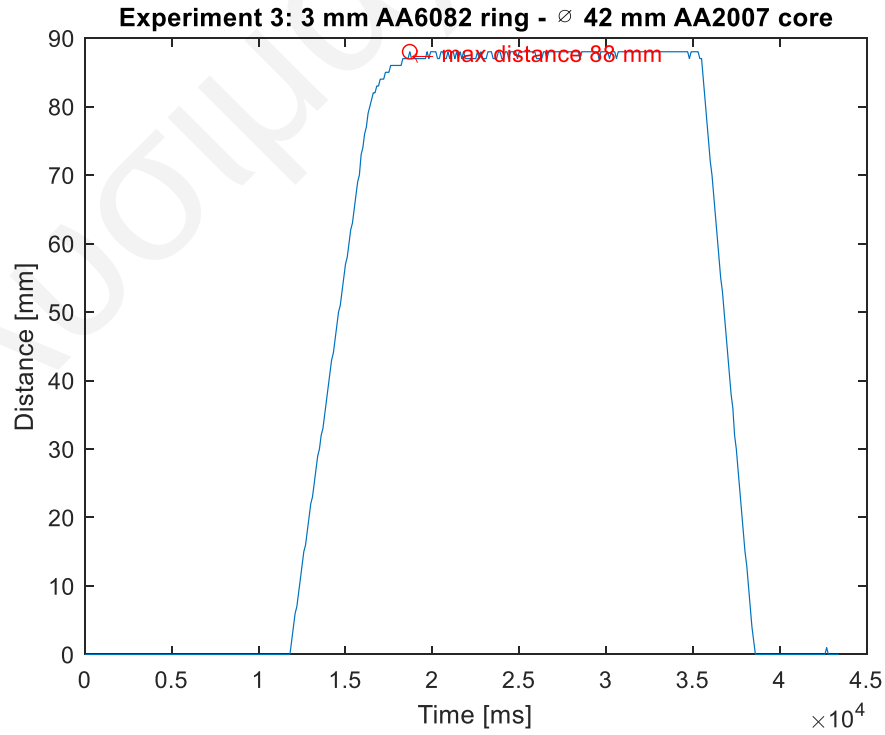

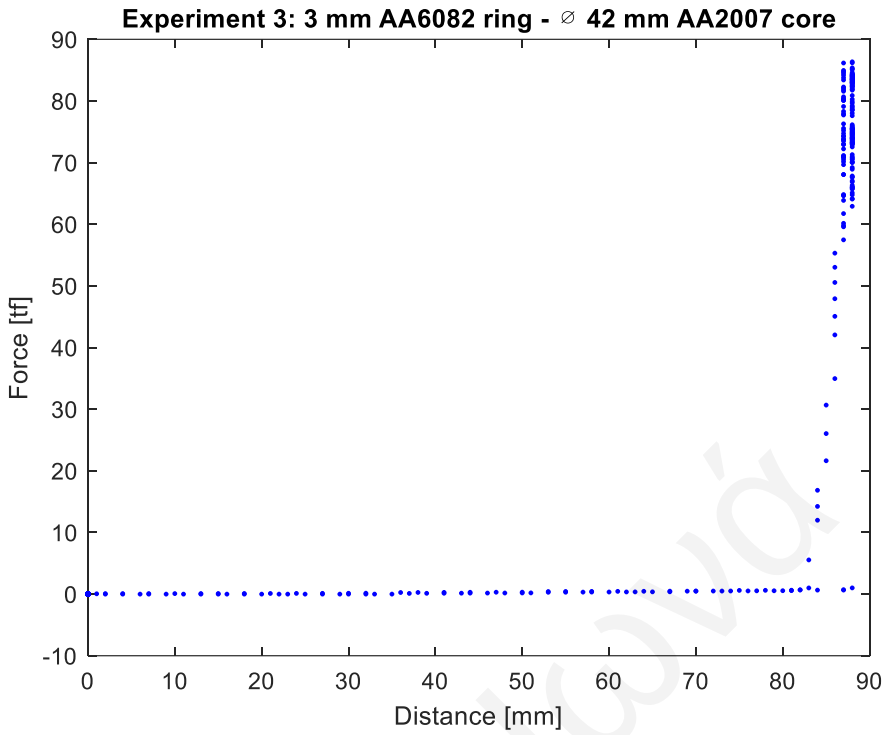

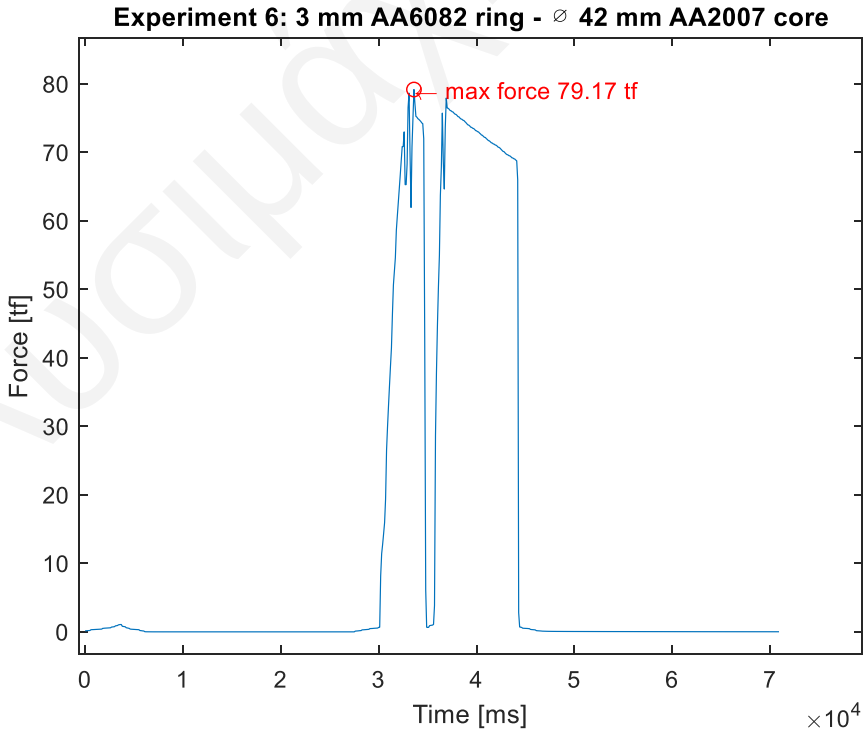

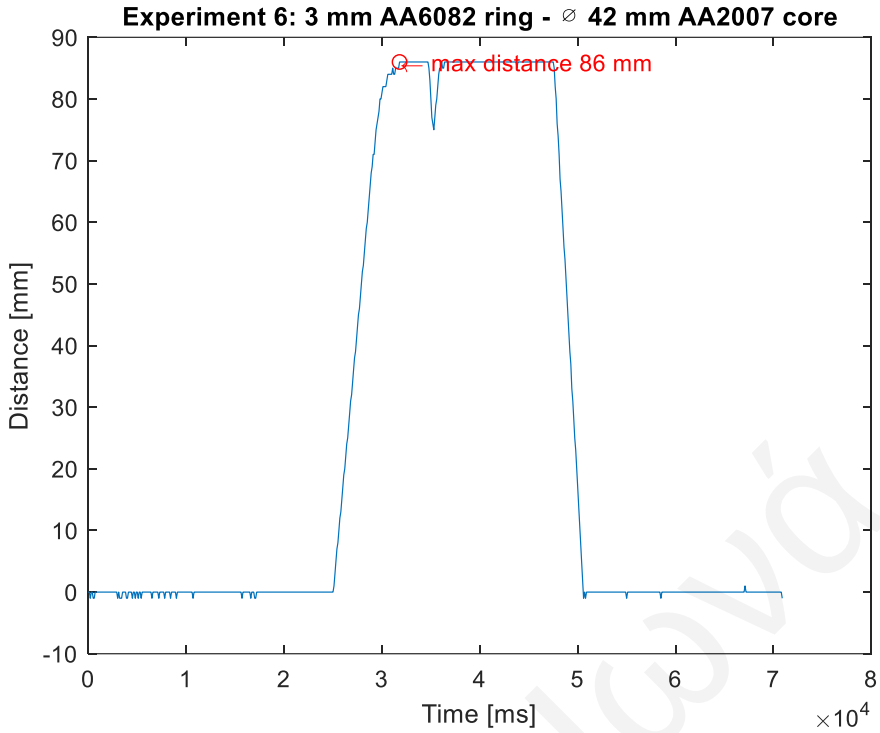

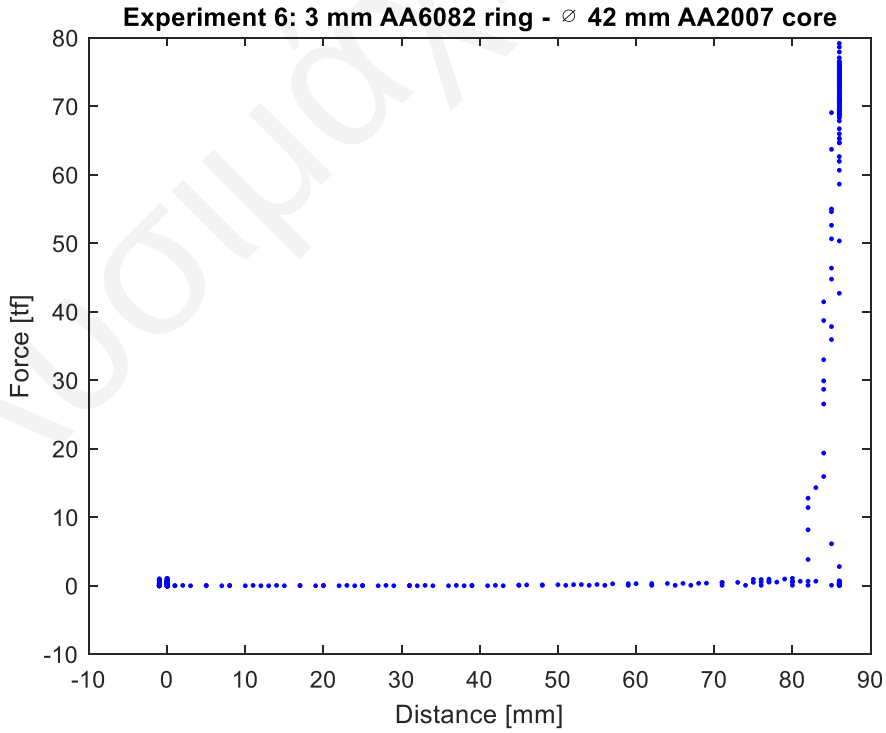

Experiment 4 and 7: 3 mm AA6082 ring - Ø42 mm AA2007 core – Cu film

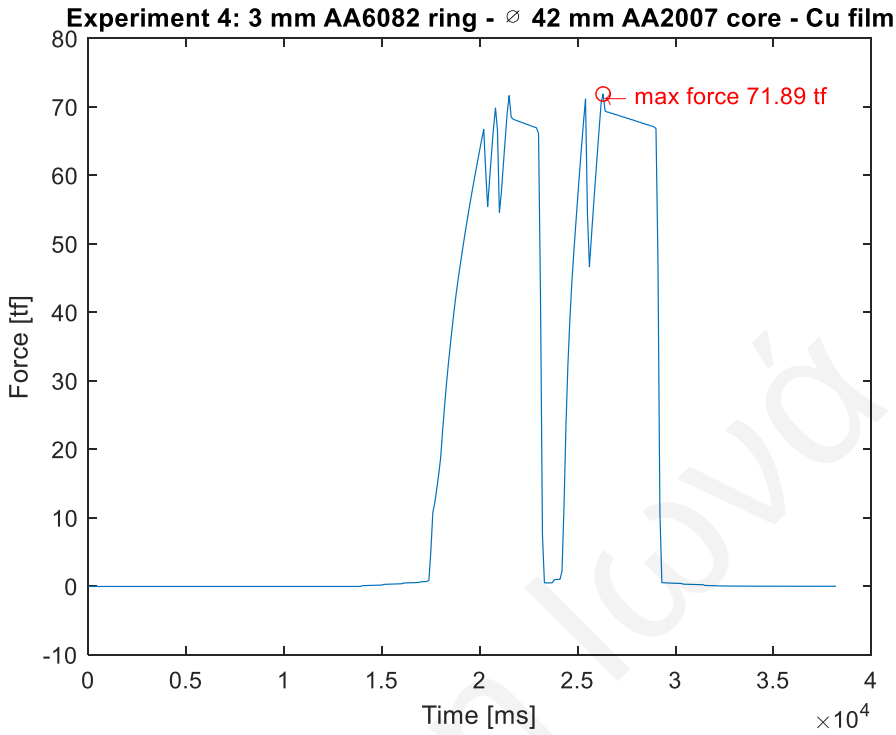

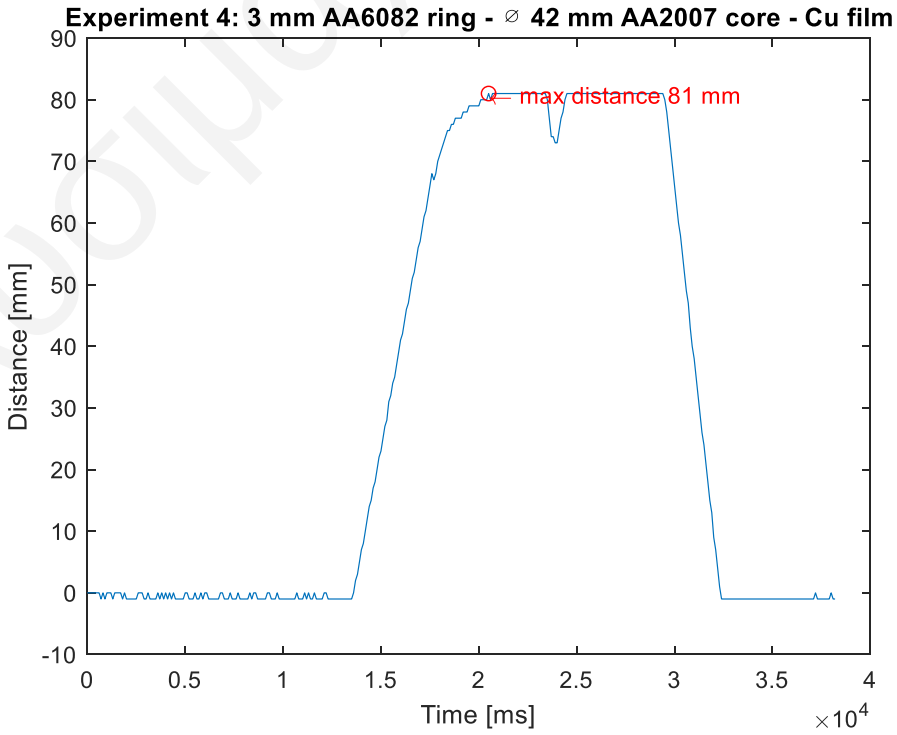

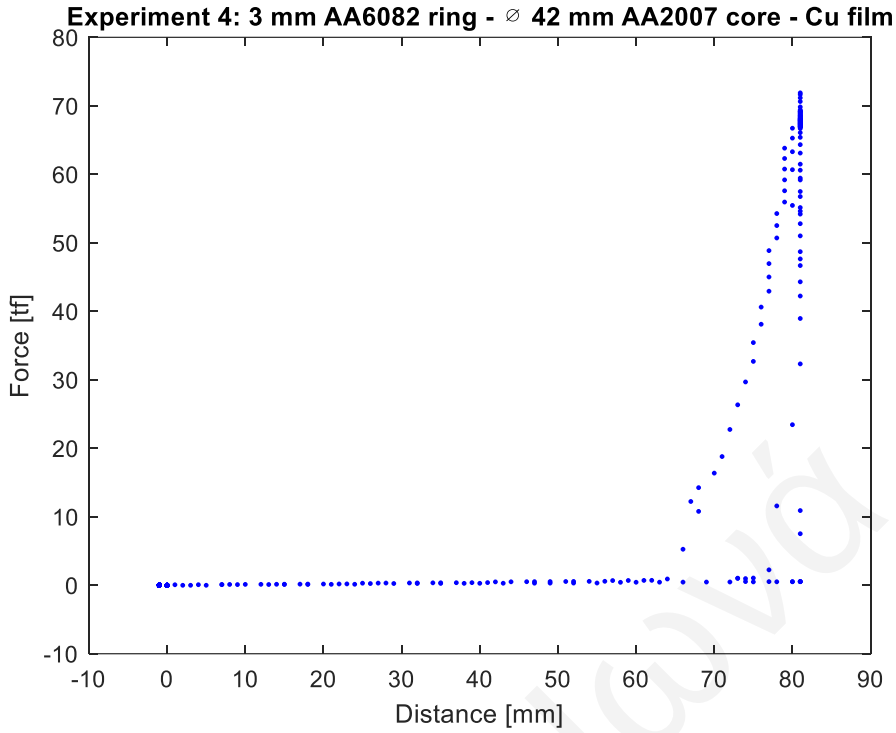

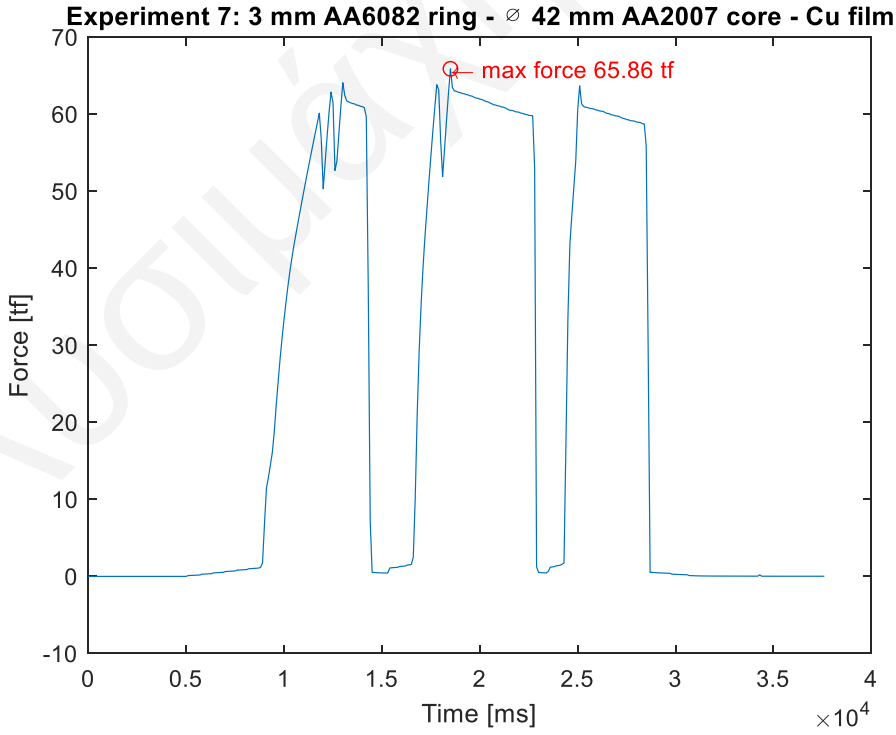

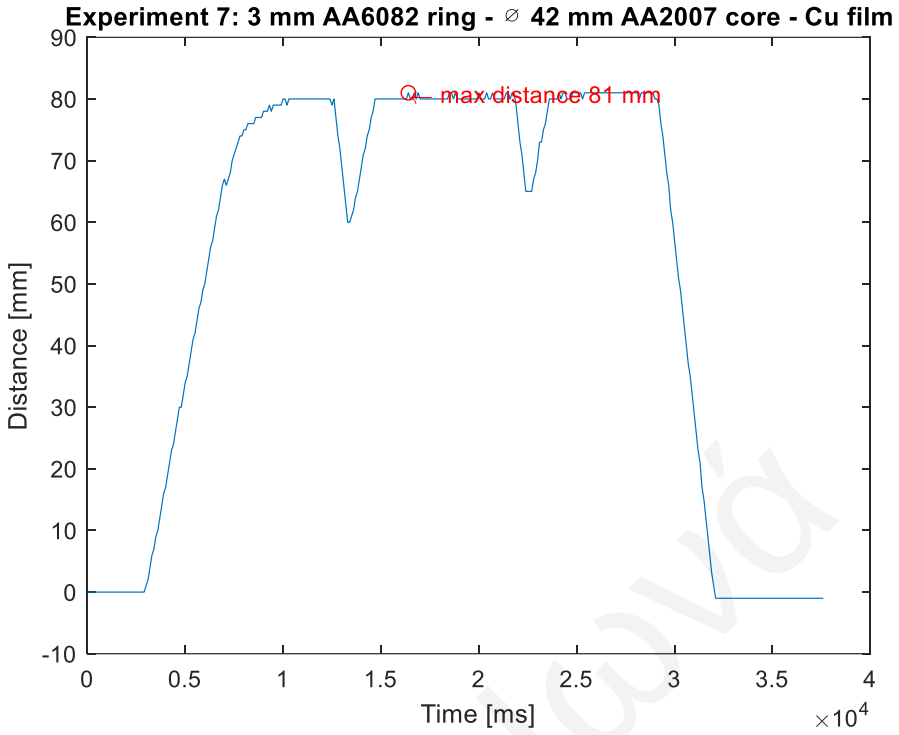

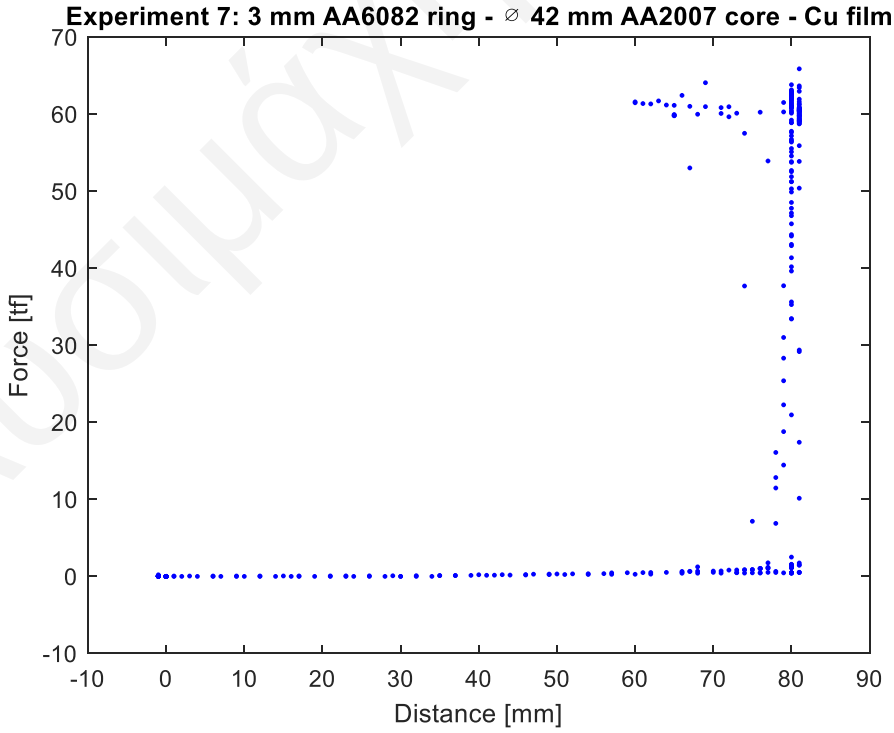

Experiment 5 and 8: 3 mm AA6082 ring - Ø42 mm AA2007 core – Ag film

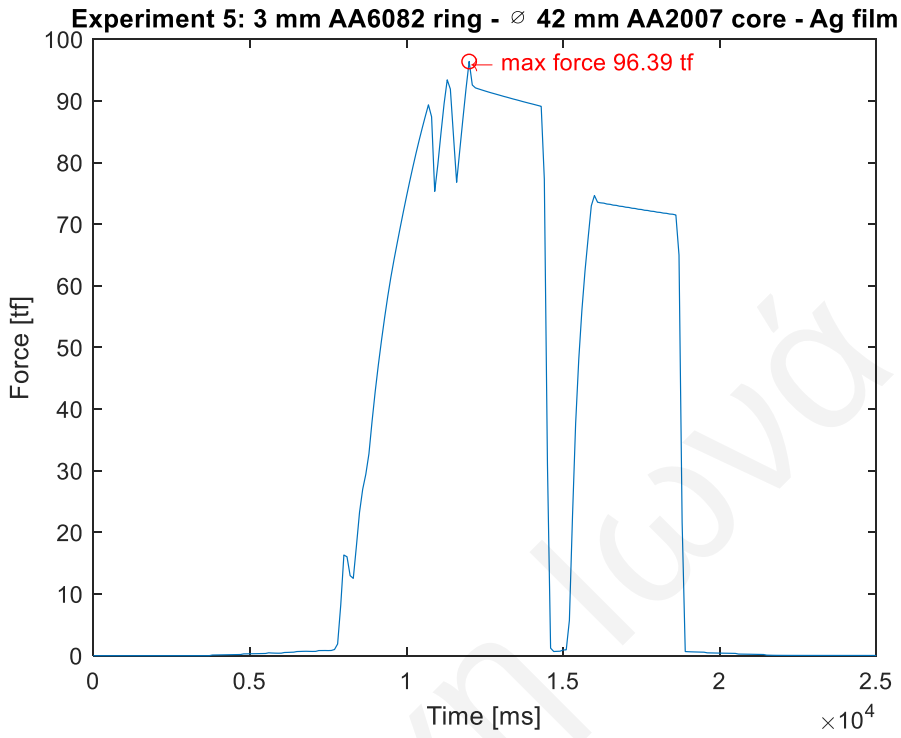

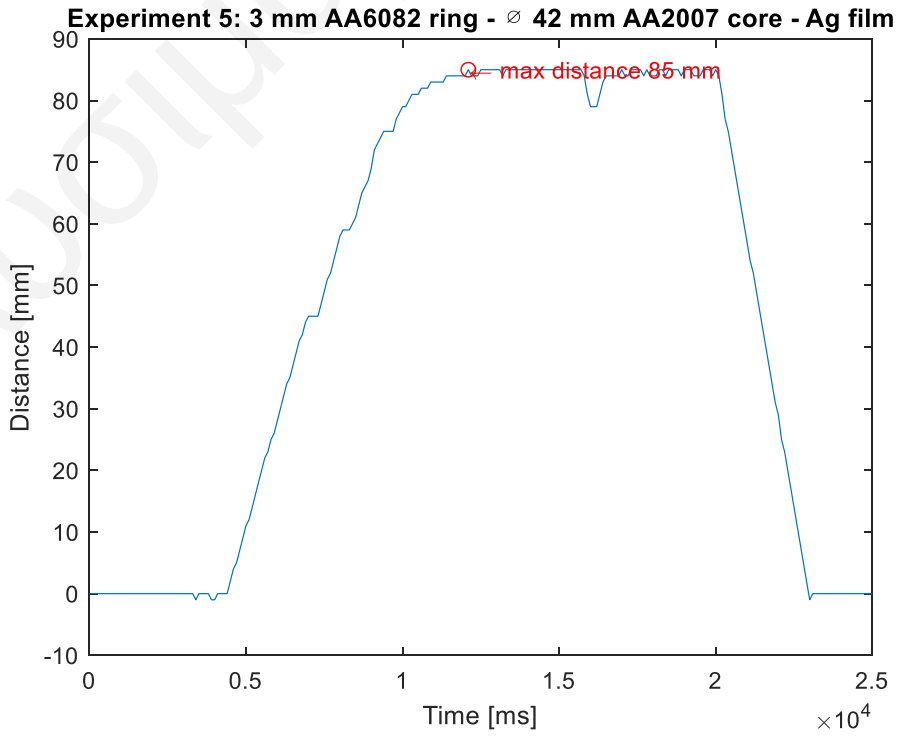

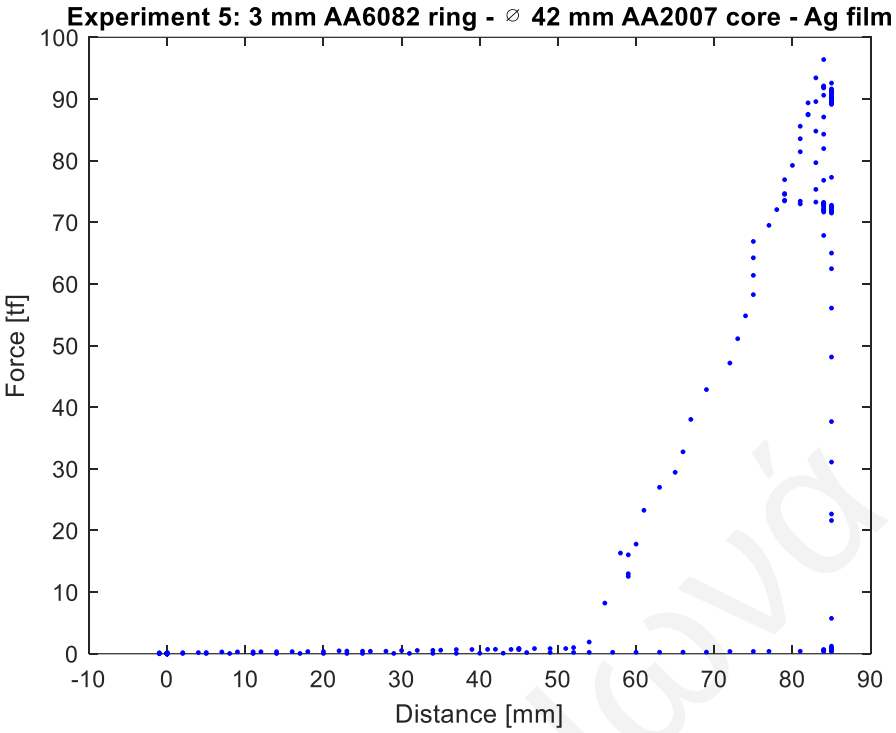

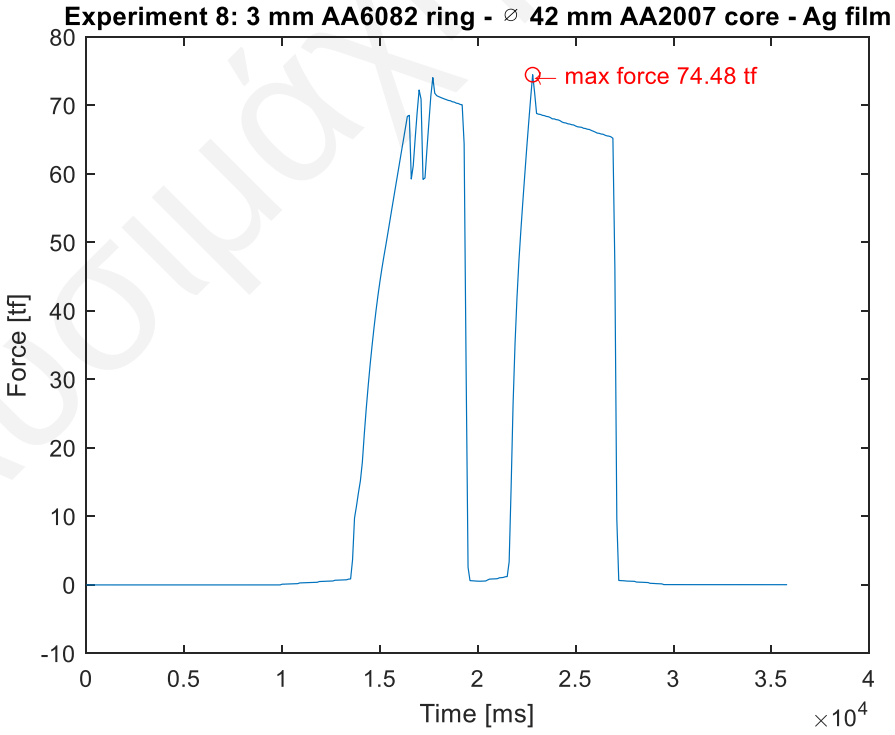

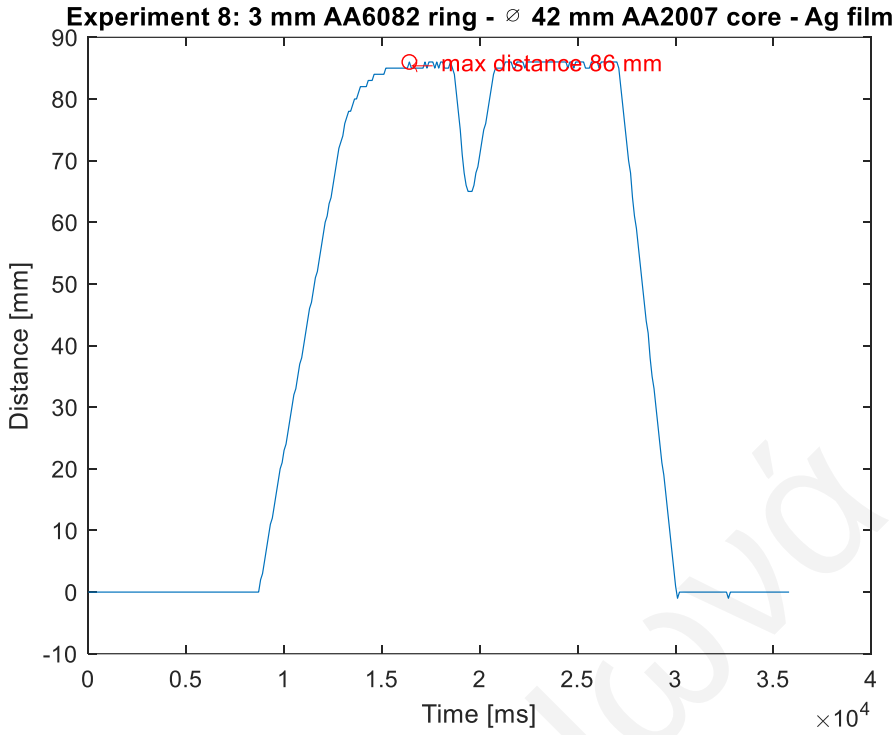

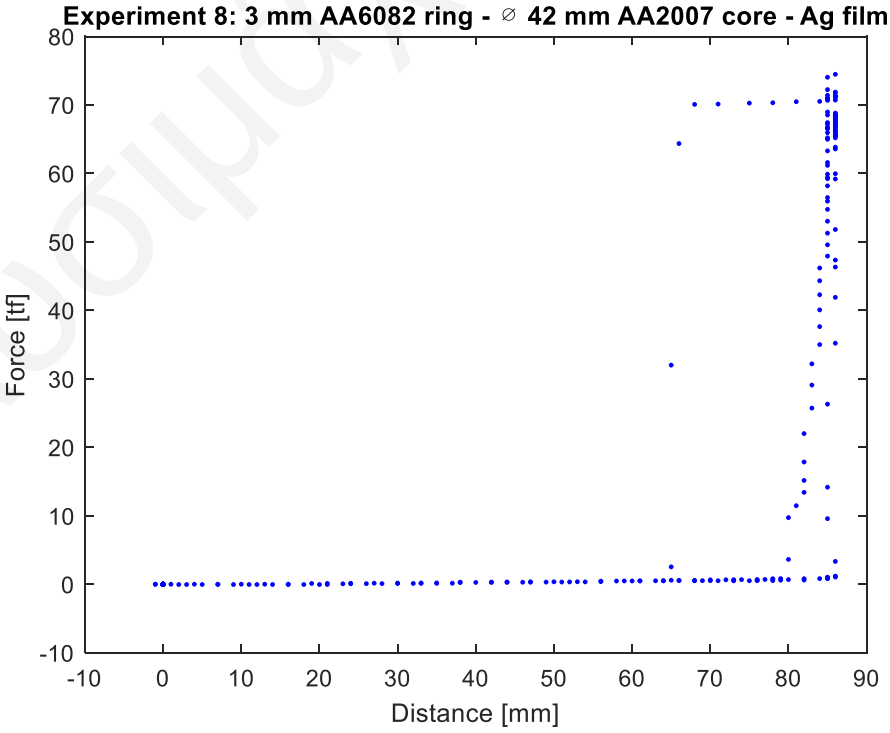

Experiment 9: 3 mm S235 ring - Ø42 mm AA6082 core – Ag film

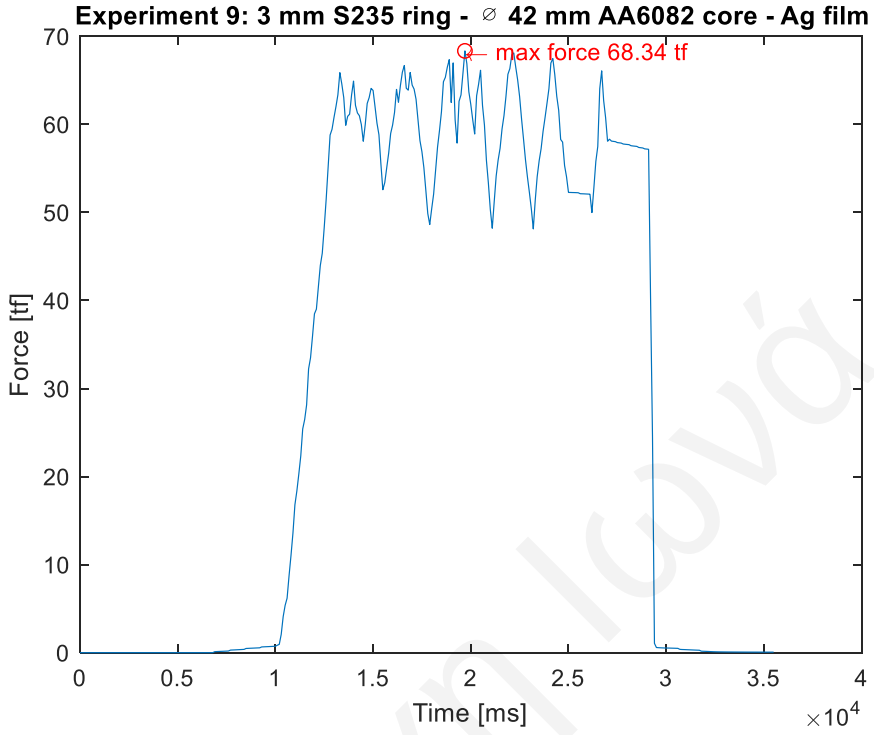

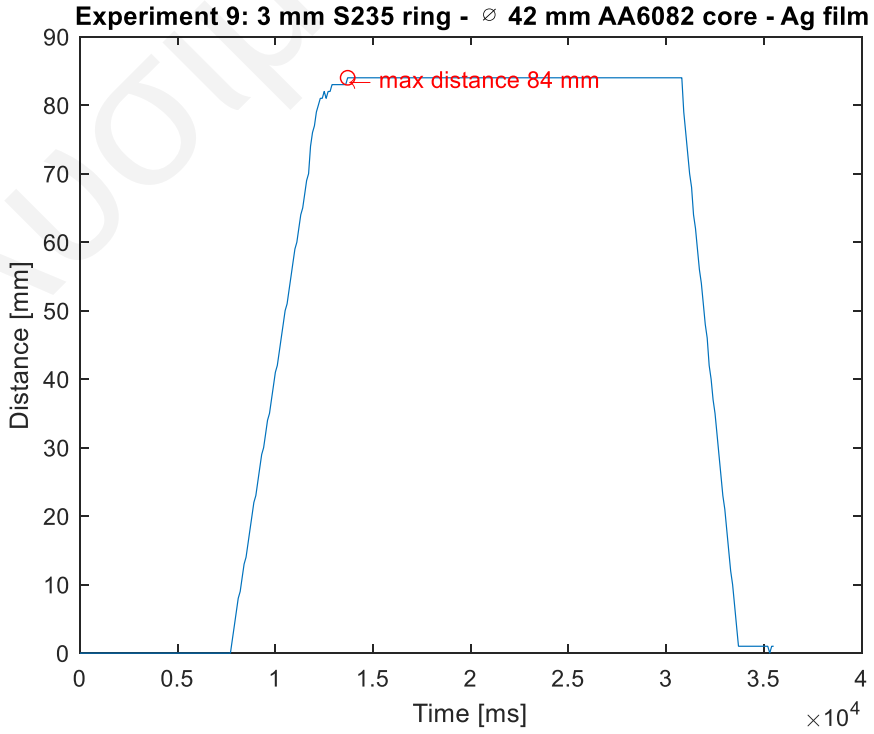

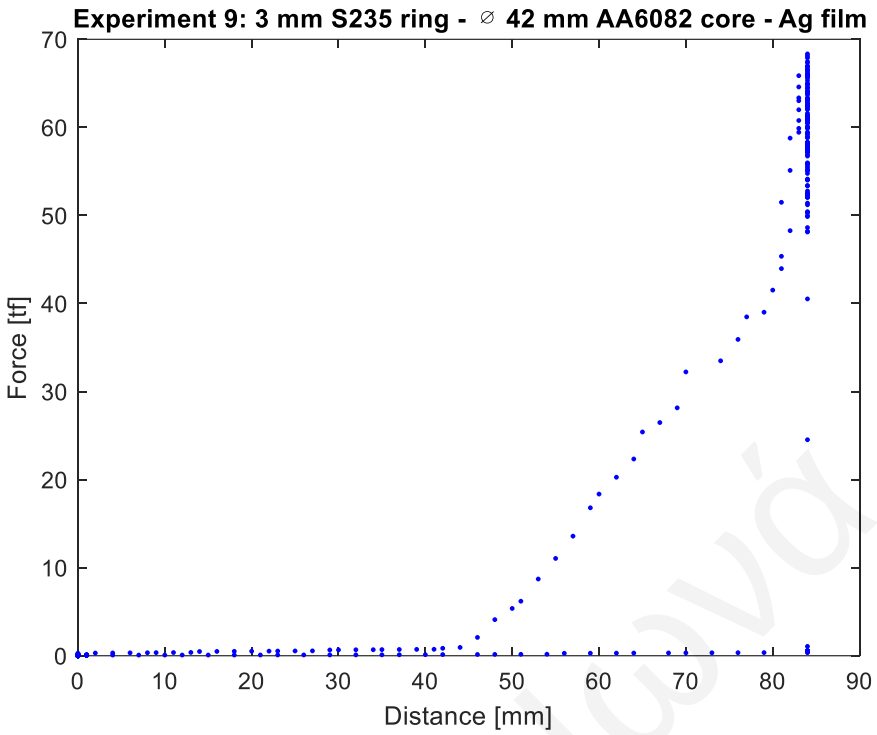

Appendix F – Vickers Hardness Measurements

Table III: Measurements taken during Micro-hardness testing of different materials

	Vickers hardness (HV)			
	Try 1	Try 2	Try 3	Average value
Gear 2: 1 mm S235 ring - ∅46 mm AA6082 core				
S235	$D_1 = 10.62\ \mu m$ $D_2 = 9.62\ \mu m$ $HV = 181.1$	$D_1 = 9.99\ \mu m$ $D_2 = 10.06\ \mu m$ $HV = 184.5$	$D_1 = 10.36\ \mu m$ $D_2 = 10.60\ \mu m$ $HV = 168.8$	$HV = 178.1$
AA6082	$D_1 = 42.35\ \mu m$ $D_2 = 47.31\ \mu m$ $HV = 92.3$	$D_1 = 46.15\ \mu m$ $D_2 = 44.24\ \mu m$ $HV = 90.8$	$D_1 = 47.53\ \mu m$ $D_2 = 45.86\ \mu m$ $HV = 85.1$	$HV = 89.4$
Gear 8:3 mm AA6082 ring - ∅42 mm AA2007 core – Ag film				
AA6082-Ag interface	$D_1 = 50.13\ \mu m$ $D_2 = 47.87\ \mu m$ $HV = 77.2$	$D_1 = 49.36\ \mu m$ $D_2 = 48.11\ \mu m$ $HV = 78.1$	$D_1 = 49.45\ \mu m$ $D_2 = 47.46\ \mu m$ $HV = 79.0$	$HV = 78.1$
AA2007-Ag interface	$D_1 = 53.90\ \mu m$ $D_2 = 51.66\ \mu m$ $HV = 66.6$	$D_1 = 54.33\ \mu m$ $D_2 = 52.87\ \mu m$ $HV = 64.5$	$D_1 = 56.66\ \mu m$ $D_2 = 52.36\ \mu m$ $HV = 62.4$	$HV = 64.5$
Ag	$D_1 = 48.94\ \mu m$ $D_2 = 50.18\ \mu m$ $HV = 75.5$	$D_1 = 49.18\ \mu m$ $D_2 = 51.61\ \mu m$ $HV = 73.0$	$D_1 = 51.81\ \mu m$ $D_2 = 51.26\ \mu m$ $HV = 69.6$	$HV = 72.7$
AA6082	$D_1 = 41.39\ \mu m$ $D_2 = 42.05\ \mu m$ $HV = 106.6$	$D_1 = 41.22\ \mu m$ $D_2 = 39.58\ \mu m$ $HV = 111.3$	$D_1 = 43.68\ \mu m$ $D_2 = 42.92\ \mu m$ $HV = 98.9$	$HV = 105.6$
AA2007	$D_1 = 47.39\ \mu m$ $D_2 = 45.40\ \mu m$ $HV = 86.2$	$D_1 = 45.05\ \mu m$ $D_2 = 46.07\ \mu m$ $HV = 89.3$	$D_1 = 47.60\ \mu m$ $D_2 = 46.57\ \mu m$ $HV = 83.6$	$HV = 86.4$
Counterpunch				
Mild steel	$D_1 = 35.90\ \mu m$ $D_2 = 25.37\ \mu m$ $HV = 197.6$	$D_1 = 30.73\ \mu m$ $D_2 = 36.76\ \mu m$ $HV = 162.8$	$D_1 = 32.19\ \mu m$ $D_2 = 29.32\ \mu m$ $HV = 196.1$	$HV = 185.5$